Sulfur isotope budget (32S, 33S, 34S and 36S) in Pacific-Antarctic ridge basalts: A record of mantle source heterogeneity and hydrothermal sulfide assimilation

J. Labidi, P. Cartigny, C. Hamelin, M. Moreira, Laure Dosso

Sulfur isotope budget (32S, 33S, 34S and 36S) in Pacific-Antarctic ridge basalts: A record of mantle source heterogeneity and hydrothermal sulfide assimilation

J. Labidi[a], [1, *,] P. Cartigny[a], C. Hamelin[b], M. Moreira[c], L. Dosso[d]

[a] Laboratoire de Géochimie des Isotopes Stables, Institut de Physique du Globe de Paris, Sorbonne Paris Cité, Univ. Paris Diderot, UMR 7154 CNRS, 1 rue Jussieu, 75238 Paris, France

[b] Centre for Geobiology, University of Bergen N- 5020, Norway.

[c] Laboratoire de Géochimie et Cosmochimie, Institut de Physique du Globe de Paris, Sorbonne Paris Cité, Univ. Paris Diderot, UMR 7154 CNRS, 1 rue Jussieu, 75238 Paris, France

[d] Centre National de la Recherche Scientifique, UMR 6538, Ifremer, BP70, 29280 Plouzané, France

****

[1] Present address : Geophysical Laboratory, Carnegie Institution of Washington, 5251 Broad Branch Rd NW, Washington DC 20015, USA

* Corresponding author : jlabidi@gl.ciw.edu

Abstract:

To better address how Mid-Ocean Ridge Basalt (MORB) sulfur isotope composition can be modified by assimilation and/or by immiscible sulfide fractionation, we report sulfur (S), chlorine (Cl) and copper (Cu) abundances together with multiple sulfur isotope composition for 38 fresh basaltic glasses collected on the Pacific-Antarctic ridge. All the studied glasses -with the exception of 8 off-axis samples- exhibit relatively high Cl/K, as the result of pervasive Cl-rich fluid assimilation. This sample set hence offers an opportunity to document both the upper mantle S isotope composition and the effect of hydrothermal fluids assimilation on the S isotope composition of erupted basalts along segments that are devoid of plume influence.

$\Delta 33S$ and $\Delta 36S$ yield homogenous values within error of Canyon Diablo Troilite (CDT), whereas $\delta 34S$ are variable, ranging between -1.57 ± 0.11‰ and $+0.60 \pm 0.10$‰ with a mean value of -0.64 ± 0.40 ‰ (1σ, vs. V-CDT). The geographic distribution of $\delta 34S$ follows a spike-like pattern, with local 34S-enrichments by up to $+1.30$‰ compared to a low-$\delta 34S$ baseline. As hydrothermal massive sulfides are characterized by relative 34S-enrichments, such first-order variability can be accounted for by hydrothermal sulfide assimilation, a process that would occur for a subset of samples (n=10). Excluding these particular samples, the mean $\delta 34S$ is significantly less variable, averaging at -0.89 ± 0.11‰ (1σ, n=28), a value that we suggest to be representative of the average MORB source value for Pacific-Antarctic basalts. Weak trends between $\delta 34S$ and 206Pb/204Pb are displayed by such uncontaminated samples suggesting the recycled oceanic crust to have a modest impact on the S budget of mantle. Their positive signs, however, suggest the depleted mantle to have a $\delta 34S$ of -1.40 ± 0.50 ‰. The sub-chondritic 34S/32S value that was previously observed for the South-Atlantic mantle is here extended to the Pacific-Antarctic domain. Such feature cannot originate from oceanic crust recycling and substantiates the concept of a core-mantle fractionation relict.

1. Introduction

Sulfur is one of the light elements entering the core composition thereby satisfying a part of its 5-10% density deficit (Birch, 1964). More than 97% of terrestrial sulfur would reside in the Earth's core (Dreibus and Palme, 1996), providing an upper estimate of 1.7 wt% S in the core (see also McDonough, 2003).

Any S isotopic fractionation between silicate and metal would lead the silicate reservoir to exhibit a ^{34}S/^{32}S shift with respect to chondrites. Since the landmark study of Thode et al. (1961), however, the sulfur (S) isotope composition of the Earth's mantle is thought to be homogeneous with a mean ^{34}S of 0.0‰, a value indistinguishable from chondrites that display an average ^{34}S of +0.04±0.31 ‰ (1 , n=24, Gao and Thiemens, 1993a,b, Orgueil excluded) with respect to CDT (consistent with the most recent estimate by Rai and Thiemens, 2007, anchored on the V-CDT scale). This statement was supported by the first published ^{34}S data of Mid-Ocean Ridge Basalts (MORB) and Ocean Island Basalts (OIB), with mean values of +0.5±0.6‰ (1 , n=18, Kanehira et al., 1973; Sakai et al., 1984; Chaussidon et al., 1991) and +0.5±0.5‰ (1 , n=6, Sakai et al., 1982) respectively. Such chondritic values were consistent with a mantle sulfur budget being dominated by chondritic late-accreted components (i.e. delivered to the Earth after core formation), a model in agreement with near-chondritic S/Se and S/Te ratios of fertile peridotite (Lorand and Alard, 2010; Wang and Becker 2013). Using an improved S extraction protocol, Labidi et al. (2012,2013) challenged this view, suggesting the depleted mantle ^{34}S to be statistically distinct from chondrites, at -1.28±0.33‰ (1).

Mantle-chondrites distinction in ^{34}S would be the consequence of a ^{34}S/^{32}S fractionation occurring during core-mantle segregation where ^{34}S-enriched sulfur would have been dissolved in the core, leading the residual mantle to be ^{34}S-deficient (Labidi et al., 2013). This previous result, however, has been obtained on basalts from the South-Atlantic ridge and it remains uncertain whether such ridge domain can be representative of the whole accessible mantle.

2

Alternatively, Cabral et al., (2013) proposed that recycled oceanic crust was characterized by a significantly negative ^{34}S (< -7‰), together with a mass-independent signature (Δ^{33}S < -0.3‰, where Δ^{33}S = ^{33}S − 1000((^{34}S + 1)$^{0.515}$ − 1)). The negative ^{34}S of the mantle could hence result from a low-^{34}S oceanic crust pervasively recycled within the MORB mantle source, following the 'marble-cake' mantle concept (Allègre and Turcotte, 1986).

In this study, we aim to address whether the ^{34}S/^{32}S shift between MORB and chondrites is a feature inherited from mantle-core equilibrium or if it instead has been acquired by crustal recycling over 4.5 Ga of Earth's history. We investigated the multiple S isotope compositions of 38 basalts dredged along two sections of the Pacific-Antarctic ridge, at 66-56°S and 53-41°S. The geochemical characteristics of these samples have been studied and their major, trace, radiogenic isotope (Sr-Nd-Hf-Pb-He) and H_2O-δD composition are reported by Vlastelic et al. (1999, 2000), Moreira et al. (2008), Hamelin et al. (2010, 2011) and Clog et al. (2013). These ridge sections are devoid of any plume influence yet using a statistical approach, Hamelin et al. (2011) showed that the source composition of the Pacific-Antarctic basalts illustrates the binary mixing between depleted mantle and recycled oceanic crust, offering the opportunity to explore the marble-cake model (Allègre and Turcotte, 1986) from the S isotope perspective.

Additionally, such basalts erupted at fast-spreading ridges extensively interact with hydrothermally altered rocks compared to melts occurring at slower spreading ridges (Michael and Cornell, 1998). Clog et al. (2013) showed that most of our samples experienced halite (or very concentrated brines) assimilations, according to their varying Cl/K ratios at a given H_2O/Ce ratio. Here, the S isotope consequence of hydrothermal rocks assimilation is addressed on the basis of Cl/K-^{34}S co-variations. Ultimately, the respective roles of hydrothermal sulfide assimilation versus recycled oceanic crust on the MORB S isotope variability are discussed.

2. Geological setting

The studied samples have been collected during two oceanographic cruises, PACANTARTIC

3

and PACANTARTIC 2, which took place along the Pacific-Antarctic ridge (PAR) between the latitude of 66-56°S and 53-41°S respectively. These ridge sections are characterized by the transition between an intermediate and fast spreading rate, from 55 mm/y at 66°S to 110 mm/y at 41°S (DeMets et al., 1990). As a consequence, the axis morphology changes from a valley to a dome north of 60°S (Géli et al., 1997; Ondréas et al., 2001; Klingelhoefer et al., 2006). Eltanin Fault System, Vacquier and Menard transform fault are the main tectonic features in this area and occur at 55, 53 and 50°S respectively (Fig. 1), and have significant impact on the trace element variability of nearby basalts (Vlastelic et al., 2000).

At high spreading-rate ridges, magma extraction is typically associated with mixing of magma pools within crustal magma chambers. Such mantle sampling leads to smoothing of its geochemical heterogeneity (Rubin et al., 2009). In contrast, off-axis magmas are formed far enough from the axis to bypass the crustal chambers system beneath the ridge and record larger mantle heterogeneity (Batiza and Vanko, 1984; Niu and Batiza, 1997; Niu et al., 2002; Brandl et al., 2012). Among the 38 PAR studied samples, 30 have been dredged at the ridge axis, the 8 others from off-axis volcanic seamounts located 10 to 300 km away from the ridge (Fig. 1 and table 1). Off-axis volcanic structures are asymmetrically, with most volcanic edifices emplaced on the Pacific plate (i.e. west of the ridge axis). According to Briais et al. (2009), such off-axis volcanism has a non-hotspot origin. It was triggered 5 My ago by a kinematic change which induced a tectonic deformation and that ultimately led to adiabatic decompression and melting of the mantle (Briais et al., 2009). The K/Ar ages of the off-axis seamounts range from 0 to 2 Ma, and are systematically younger than the crustal ages, confirming that they have been emplaced independently of the active ridge system.

3. Measurements and methods

All measurements are performed on glassy rims of pillow-lavas, as pillow interiors have been shown to display S depletion associated to post-eruptive degassing processes (Moore and Fabbi, 1971; Moore and Schilling, 1973). Major element, sulfur, chlorine and copper abundance determination were performed using an electron microprobe (EMP) on polished

4

sections with a Cameca SX100 at the CAMPARIS facility (Pierre et Marie Curie University). For Major elements and sulfur, the analytical conditions used were described in Labidi et al. (2012): 15 kV accelerating voltage, 100 nA sample current, 20 μm beam size, 10 to 60 s counting time for each point (depending on the element). Ten spots were analyzed on each polished section, and a 25 ppm 1 uncertainty is obtained for S.

For Cu and Cl, the analytical conditions used are 25 kV accelerating voltage, 500 nA sample current and 100 s counting time for each point. Here, we used the EW9309 41D-1 glass as a calibrating standard, its Cl and Cu content being both chemically determined at 55±12 ppm (1 , Bonifacie et al., 2008) and 56±10 ppm (1 , Le Roux et al., 2002), respectively. Back-scattered electron imaging has also been performed with a scanning electron microscope (SEM) in the CAMPARIS facility on all the studied glasses in order to address immiscible sulfide occurrence in our samples.

Sulfur is chemically extracted for isotopic analysis following a protocol described previously (Labidi et al., 2012), based on hydrofluoric acid processing of powdered glasses. The reader is referred to the above reference for details. After each extraction and for all samples, weighted Ag_2S precipitate is compared to S content obtained with EPM and used to determine extraction yields. Here, the chemical extraction yields an average of 102±4 % (1 , n=38). As the protocol for S extraction is strictly specific to reduced sulfur (see details in Labidi et al., 2012), such a good match with EMP supports the absence of significant amounts of oxidized sulfur in PAR MORB, in agreement with XANES spectroscopic results in worldwide samples (Métrich et al., 2009; Jugo et al, 2010).

The sulfur isotope measurements are then performed in a dual inlet MAT 253 gas-source mass spectrometer. The quality of the measurements is estimated on the basis of long-term reproducibility for IAEA reference materials. Repeated analyses versus our in-house SF_6 tank give $\bullet^{33}S$ = +0.082±0.004‰, $\bullet^{36}S$ = −0.91±0.11‰ for IAEA S1 (all 1 , n=43. $^{34}S_{S1}$ is fixed at -0.30‰ and hereafter defines the V-CDT scale) and ^{34}S = +22.33±0.06‰ (vs. V-CDT), $\bullet^{33}S$ = +0.030±0.006 ‰, $\bullet^{36}S$ = −0.17±0.07 ‰ for IAEA S2 (all 1 , n=20). CDT aliquots run versus our in-house reference gas give an average value of: ^{34}S = −0.16±0.26 ‰ (vs. V-CDT), $\bullet^{33}S$ = -0.024±0.004‰, $\bullet^{36}S$ = −0.13±0.04‰ (1 , n=11). In the following, all ^{34}S are reported against V-

CDT and all $\Delta^{33}S$ and $\Delta^{36}S$ values are recalculated and given versus our CDT measurements.

For each MORB glass sample, the S isotope measurement has been duplicated (i.e. for each sample, two aliquots of the same powder have been systematically processed). The obtained ^{34}S standard deviation between replicates is between 0.01 and 0.15‰ for all samples, with the exception of PAC2 DR34 for which the uncertainty is 0.30‰. For this sample, the extraction yields are very similar, of 94 and 96±5 %. These results are slightly lower than 100% and among the lowest of all the reported extractions in this contribution. The subsequent large uncertainty for this sample illustrates the requirement of a very efficient S extraction to insure reliable isotope results.

The standard deviation between replicates for $\bullet^{33}S$ is between 0.001 and 0.016 ‰, whereas the spectrometer yields a 0.008‰ uncertainty for a single measurement. For $\bullet^{36}S$, the typical standard deviation between replicates is between 0.008 and 0.141‰ with a spectrometer uncertainty of 0.100 ‰. These uncertainties are comparable or lower than those reported previously for a basalt standard (CH98 DR12: 0.007 ‰ and 0.106‰ for $\bullet^{33}S$ and $\bullet^{36}S$ respectively, 1 , n=12, Labidi et al., 2012).

We also report $^{206}Pb/^{204}Pb$ data for the studied off-axis basalts. The Pb isotope composition of these glasses have been determined as in Hamelin et al., (2010), and are reported in table 4.

4. Results

Multiple sulfur isotope compositions for PAR glasses are listed in Table 2. S, Cu Cl abundances of the glasses are listed in Table 3, whereas major element composition for off-axis basalts are listed in Table 4 (on-axis samples compositions are reported in Vlastelic et al., 2000 and Hamelin et al., 2010).

Small immiscible sulfides (5 microns or less in diameter) have been systematically observed in thin sections, within both on- and off-axis samples, as reported by Kanehira et al. (1973), Mathez (1976), Czamanske and Moore (1977) and Francis (1990) for other MORB. This observation demonstrates that the studied basalts are all saturated with respect to an immiscible sulfide phase across most of the magmatic differentiation. We did not observe any

6

significant trends between sulfide size/abundance and fractional crystallization indicators (e.g. MgO). Immiscible sulfide abundance never exceeded 0.5% of the bulk sulfur for each sample, i.e. > 99.5% of the sulfur is dissolved in the glass, in good agreement with previous observations (Czamanske and Moore, 1977).

S abundances within on-axis glasses vary between 930 and 1755±40 ppm whereas off-axis basalts display values between 739 and 1140±40 ppm. All these values remain nonetheless in the range of published typical MORB values (from 700 to 1800±100 ppm, Moore and Fabbi, 1971; Moore and Schilling, 1973; Mathez, 1976; Bézos et al., 2005; Le Roux et al., 2006). S amount increases with decreasing MgO (Fig. 2-A) implying an incompatible behavior of sulfur during magmatic differentiation. Such increase is however moderate compared to highly incompatible elements such as potassium (Vlastelic et al., 2000; Hamelin et al., 2010) or dissolved water (Clog et al., 2013). The well-defined FeO-S trend (Fig. 2 B) is indistinguishable from the experimental trend for FeS-saturated basalts (Carroll and Webster, 1994; Backnaes and Deubener, 2011) and confirms that all samples have sulfide at the liquidus, buffering their S abundances. Consistent with thermodynamic prediction (Gaillard and Scaillet, 2009), such saturation trend also implies that syn-eruptive sulfur degassing is negligible for our basalts, as they would otherwise be randomly shifted from this saturation line (Wallace and Edmonds, 2011). Interestingly, PAC1 DR10 plots 200±100 ppm below the saturation line (Fig. 2 B). According to its Fe-Ti-V composition, this glass is the one that has precipitated the highest amount of titanomagnetite (Hamelin et al., 2010). Among off-axis samples, PAC2 DR39-4 and PAC DR42-1c, both dredged in the northern off-axis volcanic chain, also exhibit shifts from the saturation line of 300±100 ppm and 100±100 ppm respectively (Fig 2 B). These two glasses have exceptionally high FeO contents yet with primitive MgO contents (9.69 and 11.89% FeO with 9.32 and 8.86%, respectively, see Table 4).

For on-axis samples, Cu contents range between 29 and 93±10 ppm (1), averaging at 68±13 ppm (1 , n=30). Off-axis basalts exhibit a slightly higher range, all values being between 35 and 112±10 ppm (1), averaging at 75±30 ppm (1 , n=8). The Cu abundance evolution along magmatic differentiation is presented in Fig. 3-A, along with MORB literature data (n=895). Our data fall within the MORB range, exhibiting a rough decrease with decreasing MgO.

7

Figure 4-A, B and C present the S isotope variability as a function of dredging latitude. Average δ^{33}S and δ^{36}S for the 38 studied PAR basalts are +0.010±0.005 ‰ and -0.071±0.047‰ compared to CDT, respectively (1 , Fig. 4 B and C), being strikingly homogeneous along the ridge. In contrast, the δ^{34}S variability is significant, values ranging between -1.57 to +0.60‰ (Fig. 4 A). The present dataset confirms that MORB have mostly negative δ^{34}S (Labidi et al., 2012) with the exception of only two samples that exhibit significantly positive values: the off-axis basalt PAC2 DR25-1 with a δ^{34}S of +0.35±0.06‰, and the on-axis glass PAC2 DR20-1 with a δ^{34}S of +0.60±0.10‰. The mean δ^{34}S for on-axis basalts is -0.64±0.40 ‰ (1 , n=30) whereas off-axis average is -0.82±0.56 ‰ (1 , n=8).

Samples cluster around a low- δ^{34}S baseline that appears to shift from   -0.80±0.10 ‰ south of 45°85'S to   -1.10±0.10‰ north of 45°85'S (Fig. 4A). Among the 30 on-axis samples, 21 lie within this baseline, whereas 9 basalts exhibit systematically higher δ^{34}S representing +0.35 to +1.40‰ deviations with respect to the isotope baseline. S isotope distribution for off-axis basalts follows a comparable pattern: south of 45°85'S, their minimal δ^{34}S is between -0.82 and -0.70‰, whereas it is between -1.25 and -1.12‰ north of 45°85'S. Only the sample PAC2 DR42-1c exhibits a lower value than the on-axis baseline, with a δ^{34}S of -1.57 ± 0.08‰. PAC2 DR25-1 displays a δ^{34}S of +0.35±0.06‰ that represents a +1.15‰ deviation with respect to the on-axis baseline.

Chlorine abundances vary between 20 and 2163±10 ppm (1 , Fig. 5-A), within the MORB range (Michael and Cornell, 1998), with an average value of 428±488 ppm for on axis basalts (1 , n=30, Table 3). In comparison, off-axis samples have generally lower Cl contents, with a mean value of 96±107 ppm (1 , Fig. 5-A). The Cl/K ratios of on-axis basalts vary between 0.06 and 0.71, with an average of 0.28±0.16 (1 , n=30), which is significantly higher than the expected value for uncontaminated basalts (Cl/K < 0.08, Michael and Cornell, 1998). Therefore, Cl/K systematics highlight that almost all on-axis basalts have assimilated Cl-rich contaminants (Fig. 5-B, Clog et al., 2013). Off-axis Cl/K ratios are lower, between 0.04 and 0.11 with a mean value of 0.08±0.03 (1 , excluding PAC2 DR25-1), illustrating the least-contaminated basalt features (Fig. 5 B).

^{206}Pb/^{204}Pb ratios of off-axis samples significantly overlap the on-axis range, with values

8

between 18.560 to 19.537 (Table 4). This range is nonetheless extended towards higher [206]Pb/[204]Pb ratios, illustrating higher HIMU contributions sampled by off-axis basalts.

5. The S-abundance systematic in MORB

Average abundances for all major elements between the two sections are indistinguishable at a given MgO, implying similar depths and rates of melting (see Vlastelic et al., 2000, Hamelin et al., 2010). It is worth noting that among on-axis basalts, 4 of them exhibit a significant drop in Fe, Ti and V contents at a given MgO (Vlastelic et al., 2000; Hamelin et al., 2010; Clog et al., 2013; Fig. 6). These samples are the most differentiated, having MgO abundances < 5%. These observations are consistent with triggering of titanomagnetite precipitation occurring after its appearance on the liquidus, buffering the Fe, Ti and V abundances in melts (Jenner et al., 2010; Lee et al., 2012).

Off-axis basalts have MgO contents between 9.32% and 7.77% whereas on-axis basalts are between 8.18% and 3.86% (table 4). Such relatively primitive compositions illustrate shorter residence times in magmatic chambers for off-axis liquids compared to on-axis basalts. Na_2O and P_2O_5 abundances at a given MgO are similar for on- and off-axis basalts (Table 4). However, CaO and Al_2O_3 contents of off-axis basalts are different from typical on-axis values. The CaO contents of off-axis samples are lower than those of on-axis samples at a given MgO, whereas their Al_2O_3 contents are relatively high. FeO contents are broadly similar to the on-axis trend except for two samples: PAC2 DR39-4 and DR42-1c, which respectively contain 11.89% and 9.69% FeO for a primitive MgO of 8.86% and 9.32% (Table 4). The origin of such values remains unclear but was interpreted by Brandl et al. (2012) to reflect a heterogeneous upper mantle on the melting-region scale, beneath an East-Pacific ridge seamount.

5.1. Sulfur speciation and implications for MORB fO_2

Our extraction procedure being strictly specific to reduced sulfur (see details in Labidi et al., 2012), extraction yields averaging at 102±4% (1 , n=38) demonstrates that sulfur is only dissolved under its reduced form. Previous MORB fO_2 measurements have been constrained via the Fe^{3+}/Fe_{Total} ratio (Christie et al.,1986; Bézos and Humler, 2005; Cottrell and Kelley,

9

2011), but led to contradictory estimates, from FMQ -1.5±0.5 (n=78), FMQ -0.41±0.43 (n=104) to FMQ +0.10±0.18 (n=103, all 1), respectively. Because sulfur speciation in a basalt glass depends upon the oxygen fugacity, our results can bring constraint on the MORB fO_2. The transition from S^{2-} to S^{6+} occurs between FMQ and FMQ +2 (Métrich et al., 2009; Jugo et al., 2010). For PAR basalts, independently of any Fe^{3+}/Fe_{Total} measurement, the sulfur speciation provides a robust upper limit of MORB fO_2 at FMQ -0.20±0.20, in agreement with Christie et al. (1986) and Bézos and Humler (2005).

5.2. Sulfide fractionation along partial melting and magmatic differentiation

Sulfur abundance coinciding with sulfur solubility (Mavrogenes and O'Neill, 1999), which is reflected by the well-defined FeO-S trend (Fig. 2-B), illustrates sulfide saturation across magmatic differentiation, consistent with the ubiquitous occurrence of magmatic sulfide in thin sections (quantification in sections 5.2.1 and 5.2.2). The occurrence of immiscible sulfides in the most primitive samples highlights the possibility that PAR basalts were already FeS-saturated in their melting zone. Multiple independent lines of evidence indicate that MORB are saturated at melting depths, and that they may remain S-buffered until eruption. First, sulfur abundance systematics in abyssal peridotite predict 200±40 ppm sulfur in the fertile MORB-source mantle (Luguet et al., 2003; Lorand et al., 2013). Sulfur being incompatible in silicates, a   10% extent of melting should lead to 2000 ppm S in the produced melt, to be compared with sulfur solubility in primitive MORB (8 wt% FeO) of 900±100 ppm (Mavrogenes and O'Neill, 1999). Partial melts produced after 10% melting should therefore accommodate less than 50% of the available sulfur and leave more than 50% of initial S in residual mantle (see also Keays, 1995). Consistently, worldwide abyssal peridotites systematically contains residual sulfide (Luguet et al., 2001, 2003; Harvey et al., 2006; Seyler et al., 2007). Experimental studies have established the negative pressure dependence of S solubility in MORB (Mavrogenes and O'Neill, 1999; O'Neill and Mavrogenes, 2002): upon decompression and adiabatic ascent, a S-saturated magma could cross S undersaturation line. The systematic occurrence of disseminated sulfides of magmatic origin in ophiolitic lherzolites (Ligurides, Italy, Sumail and Maqsad, Oman) however supports the idea that basaltic liquids may remain S-

10

saturated during their ascent into magmatic chambers (Lorand 1987, 1988; Luguet et al., 2004). In this context, the role of fractional crystallization is the key to keep the magma saturated and precipitating sulfides (Holzheid and Grove, 2002). Saturation with sulfide along the entire magmatic differentiation (during melting, most likely during ascent, and during later differentiation stages in shallow magma chambers) therefore precludes constraining S content and its possible variability in MORB mantle source. Yet S/Dy ratio has been used by Saal et al. (2002) and Arevalo and McDonough (2010) to provide a MORB mantle S estimate of 146±35 ppm (see also Shaw et al., 2010, for the peculiar case of Gakkel ridge). Such sulfur content normalization to an un-buffered incompatible element leads to an underestimation of the mantle sulfur content. This likely explains the discrepancy between mantle S-contents of 146±35 ppm (Saal et al., 2002; Arevalo and McDonough, 2010) inferred from S/Dy systematics compared to 200±40 ppm estimates obtained from peridotite studies (Luguet et al., 2003; Lorand et al., 2013).

Three basalts nonetheless offset the FeO-S trend, and have to be treated separately. Among off-axis samples, PAC2 DR39-4 and PAC DR42-1c are shifted by 300±100 ppm and 100±100 ppm, respectively (Fig. 2-B), and are those with unusually high Fe-contents (11.89 and 9.69 wt% FeO for 8.86 and 9.32 wt% MgO, respectively, Table 4). It is emphasized that these two samples contain sulfide blebs, highlighting that they define a distinct saturation line, possibly in relation with a distinct Fe speciation, temperature or pressure of equilibration.

Among on-axis basalts, PAC1 DR10-1g exhibits a 200±100 ppm shift with respect to the FeO-S trend. Again, not only is this glass sulfide saturated, but it also belongs to the most-differentiated basalts (together with PAC2 DR06-6, PAC2 DR20-1 and PAC2 DR27-1) displaying low V, Ti and Fe amounts with respect to the trend defined by other samples (Fig. 6, Vlastelic et al., 2000; Hamelin et al., 2010) illustrating magnetite precipitation. We observe that the magnetite fractionation triggers a Fe drop in basalts without impacting S solubility (i.e. S amount at a given FeO), except for PAC1 DR10-1g (comparable observations have recently been made on other differentiated MORB by Jenner et al., 2012). This particular glass exhibits the lowest V-Fe-Ti amount for a given MgO among the most differentiated basalts, displaying the highest efficiency of magnetite fractionation. However magnetite has a $Fe^{3+}/Fe_{Total} > 0.5$

11

such that its fractionation efficiency lowers the Fe^{3+}/Fe_{Total} of melts (Kelley and Cottrell, 2012; Lee et al., 2012). Here, we suspect the associated change in fO_2 to result in a lowering of S solubility (Wallace and Carmichael, 1992).

5.2.1 Sulfide fractionation quantification: Method 1

The modeled curve in Fig. 2-B corresponds to the predicted S MORB content ($S_{predicted}$) following simple crystal fractionation laws calculated using the MELTs software assuming an incompatible bulk partition coefficient ($D_{sil-liq}=10^{-3}$) for S. The difference between this curve and the measured S in MORB corresponds to the amount of fractionated sulfides (Fig 2-B). The remaining fraction of sulfur can be calculated as follows:

$$f_{sulf} = S_{measured}/S_{predicted} \qquad (1)$$

f_{sulf} varies between 0.93 and 0.23 for studied basalts (Table 3), smoothly decreasing with ongoing magmatic differentiation. The following regression has been computed to estimate f_{sulf} at a given FeO:

$$f_{sulf} = -0.01 \times FeO^2 + 0.17 \times FeO + 0.15 \qquad (2)$$

The mass of segregated sulfide can also be estimated. For this, we define S_{loss} as the mass of sulfur being fractionated during the magmatic differentiation. Regression of S_{loss} gives the following equation:

$$S_{loss} = 2.36 \times FeO^2 - 40.79 \times FeO + 194.38 \qquad (3)$$

where S_{loss} is in mg S for 100g of initial liquid and FeO is in wt%. In this calculation only samples having MgO > 5% have been used as for lower values, the decrease in FeO associated to magnetite fractionation prevents this calculation to be performed. Assuming these magmatic sulfides are of FeS composition (Francis, 1990; Roy-Barman et al., 1998), the average mass proportion of sulfide in the bulk minerals fraction is calculated to be 0.19±0.07 wt%.

5.2.2. Sulfide fractionation quantification: Method 2

The amount of sulfide fractionation can also be computed from copper amounts in MORB. Cu behaves as an incompatible element in the absence of magmatic sulfide (Jenner et al., 2010;

12

Lee et al., 2012) with $D_{sil-liq} = [Cu]_{sil}/[Cu]_{liq} < 10^{-1}$, close to heavy rare earth element partition coefficients, predicting a Cu content increase with decreasing MgO. However, Cu abundance roughly decreases in MORB (Fig. 3-A) constraining the *bulk* partition coefficients $D_{min-liq}$ (where min refers as bulk minerals, including silicates and sulfides) to be higher than unity, estimated here at 1.4±0.2 (see Fig 3-A and Bezos et al., 2005). Cu being chalcophile (i.e. having a $D_{sulf-liq}$ = $[Cu]_{sulf}/[Cu]_{liq}$ much higher than 1), such decrease signs sulfide fractionation. Cu abundance can be described using crystal fractionation laws as follows:

$$[Cu]_{liq} = [Cu]_{initial} \acute{}\ f^{D^{min-liq}-1} \quad (4)$$

where f is the remaining mass fraction of liquid. $D_{Cu}^{min-liq}$ is expressed as follows:

$$D_{Cu}^{min-liq} = X_{sil} \acute{}\ D_{Cu}^{sil-liq} + X_{sulf} \acute{}\ D_{Cu}^{sulf-liq} = 1.4 \quad (5)$$

where X_{sil} and X_{sulf} are mass fractions of silicate and sulfide minerals respectively, considering that:

$$X_{sil} + X_{sulf} = 1 \quad (6)$$

Combining equations 6 and 5 leads to the following simplification where the only unknown is X_{sulf}:

$$D_{Cu}^{min-liq} = \left(1 - X_{sulf}\right) \acute{}\ D_{Cu}^{sil-liq} + X_{sulf} \acute{}\ D_{Cu}^{sulf-liq} = 1.4 \quad (7)$$

$D_{Cu}^{sil-liq}$ and $D_{Cu}^{sulf-liq}$ are taken as 10^{-1} (Lee et al., 2012) and between 300 and 1200 (MacLean and Shimazaki, 1976; Rajamani and Naldrett, 1978; Lynton et al., 1993; Gaetani and Grove, 1997; Ripley et al., 2002), respectively. Assuming that the sulfide exsolution occurs under chemical equilibrium across the whole magmatic differentiation with constant $D_{Cu}^{sil-liq}$ and $D_{Cu}^{sulf-liq}$, equation (7) allows the calculation of X_{sulf}.

Modeling the Cu-MgO trend can be improved by normalizing the Cu abundance to an element having a comparable $D_{sil-liq}$ such as yttrium, which has a $D_{sil-liq}$ = 0.088 (Workman and Hart, 2005) close to the estimate of Lee et al. (2012) for copper. Cu/Y ratios decrease smoothly with decreasing MgO (fig. 3-B), further confirming sulfide fractionation. Y behavior can be described as follows:

13

$$D_Y^{min-liq} = X_{sil} \cdot D_Y^{sil-liq} + X_{sulf} \cdot D_Y^{sulf-liq} = 0.088 \quad (8)$$

where $D_Y^{sulf-liq}$ is negligible, giving $D_Y^{sil-liq} = D_Y^{min-liq}$, and:

$$D_{Cu}^{sil-liq} = D_Y^{min-liq} = 0.088 \quad (9)$$

Crystal fractionation laws give:

$$\frac{Cu}{Y} = \left(\frac{Cu}{Y} \right)_{initial} \cdot \frac{f^{D_{Cu}^{min-liq}-1}}{f^{D_Y^{min-liq}-1}} \quad (10)$$

that becomes :

$$\frac{Cu}{Y} = \left(\frac{Cu}{Y} \right)_{initial} \cdot f^{D_{Cu}^{min-liq} - D_Y^{min-liq}} \quad (11)$$

Ultimately leading to:

$$\frac{Cu}{Y} = \left(\frac{Cu}{Y} \right)_{initial} \cdot f^{D_Y^{sil-liq} + X_{sulf} \cdot (D_{Cu}^{sulf-liq} - D_Y^{sil-liq})} \quad (12)$$

X_{sulf} can be calculated at a known $D_{Cu}^{sulf-liq}$ and a given Cu/Y. For a $D_{Cu}^{sulf-liq}$ of 900 (Ripley et al., 2002; Lee et al., 2012), the decreasing trend observed in Fig. 3 B is fitted if 0.19±0.04 wt% minerals crystallizing are sulfides. Although independent from the S-abundance systematics, this Cu/Y-derived estimate is consistent with the method 1 (0.19±0.07 wt%, see section 5.2.1). However we note that if the REE-homogeneous source of PAR basalts allows this calculation to be undertaken (Hamelin et al., 2010), this method is very sensitive to Y abundances in primitive magmas and should be approached with caution in other, more heterogeneous, localities.

6. On a viable explanation for the S isotope variability in MORB

Large-scale source variation with a smooth northward increase of HIMU component contribution cannot explain the 'spike-like' increase in [34]S that seems randomly distributed along the ridge (Fig. 4 A). In this section, we discuss the origin of the 2.2‰ variability in [34]S/[32]S in terms of sulfide fractionation and hydrothermal sulfide assimilation.

Only PAC1 DR12-1g and PAC1 DR13-2g exhibit anomalous Nd-Hf isotope compositions that are not satisfied by the binary mixing between HIMU and depleted mantle (Hamelin et al.,

14

2011). These two samples have ^{34}S of -0.31±0.02‰ and -0.65±0.10‰, significantly higher than the isotope baseline recorded in the 66-56°S locality. Small-scale source heterogeneity cannot be excluded to account for their anomalous ^{34}S and therefore, they are left aside from the following discussion.

6.1. Progressive ^{34}S/^{32}S fractionation along sulfide exsolution: Model A

Progressive sulfide fractionation may induce δ^{34}S variation owing to ^{34}S/^{32}S fractionation between FeS$_{dissolved}$ (i.e. in silicate melt) and FeS$_{immiscible}$ (i.e. sulfide liquid). The $^{34}a_{dissolved-exsolved}$ value can be estimated by exploring relations between ^{34}S and sulfide exsolution proxies. A weak trend seems to appear, as the more differentiated is a basalt, the higher is its ^{34}S. In a ^{34}S-f$_{sulf}$ plot (Fig. 7), R^2 is 0.54 for all on-axis samples and decreases significantly to 0.20 when the magnetite-fractionated samples are excluded. It is noted that when off-axis samples are added, R^2 drops below 0.10. Similar conclusion holds for ^{34}S vs. Cu/Y relationships. At odds with the conclusion of Chaussidon et al. (1989) that $^{34}a_{dissolved-exsolved}$ = 0.997±0.003 (predicting a ^{34}S decrease of residual melts as sulfide exsolution proceeds), such a rough trend would require the exsolved sulfide to be enriched in lighter isotopes. The rough trend observed in Fig. 7 can be fitted using equation 13 with a $^{34}a_{dissolved-exsolved}$ = 1.00115 with initial ^{34}S of -1.20‰ (details in Fig. 7 and its caption).

Because sulfur in the most primitive MORB is the product of a partial dissolution occurring during partial melting, a non-negligible ^{34}S/^{32}S fractionation between dissolved S and immiscible sulfides would imply that MORB ^{34}S does not represent the value of their mantle source: For 10% melting, 200 ppm S in the mantle and 900 ppm S solubility in MORB, 55% S would remain in the mantle (Keays, 1995; Mavrogenes and O'Neill, 1999). The initial MORB ^{34}S value at -1.20‰ (Fig. 7) would be inherited from this first equilibrium between dissolved and residual sulfide. Under batch equilibrium melting and for a $^{34}a_{dissolved-exsolved}$ = 1.00115, the fertile MORB source ^{34}S is predicted to be lower than MORB values, at ~ -1.80‰.

15

With $^{34}a_{dissolved-exsolved}$ = 1.00115, melting variations could produce ^{34}S variability at a given f_{sulf}, possibly explaining the ^{34}S/^{32}S deviations from the main trend of Fig. 7. However, melting-induced ^{34}S/^{32}S fractionations could only produce +0.5‰ variations, at most (see caption of Fig. 7). Therefore, such model cannot account for the observed ^{34}S-enrichments in some samples with respect to the main trend (up to +1.30‰, Fig. 7).

In addition, such isotope fractionation under magmatic temperature is unexpectedly high (Taylor, 1986; Ohmoto and Goldhaber, 1997) in particular as no S-reduction/oxidation reaction occurs during sulfide exsolution. To the best of our knowledge, $^{34}a_{immiscible-dissolved} = {}^{34}R_{immiscible} / {}^{34}R_{dissolved}$ (with ^{34}R being ^{34}S/^{32}S ratio) has never been experimentally determined, but it is known that at equilibrium and high temperature (T> 850°C), S isotope fractionation is significant (> 1‰) only if associated with redox processes (Taylor, 1986; Ohmoto and Goldhaber, 1997, Sakai, 1968; Richet et al., 1977; Ohmoto, 1979; Ono et al., 2007; Otake et al., 2008). This is supported by other studies of natural samples which indicates $^{34}a_{dissolved-exsolved} \approx 1.000$ at magmatic temperature (Mandeville et al., 1998;2009). A negligible S isotope fractionation during sulfide precipitation is also consistent with the preservation of correlations between source tracers (e.g. ^{87}Sr/^{86}Sr) in samples from the South-Atlantic ridge (Labidi et al., 2013). An alternative model must be implemented to account for the ~2.2‰ ^{34}S/^{32}S variability in PAR basalts.

6.2. An alternative model

Cl/K ratios of on-axis PAR glasses (0.28±0.16, 1) provide evidence of seawater-derived fluid assimilation (Fig. 5, Michael and Cornell, 1998, Clog et al., 2013). This process scales here with magmatic differentiation (Fig. 5-B), as previously observed in MORB from the East-Pacific ridge and the Galapagos spreading center (Michael and Cornell 1998). This is because differentiation implies longer residence times in crustal magma chambers, especially in fast-spreading ridges (Michael and Cornell, 1998), hence allowing increased crustal assimilation throughout differentiation of PAR basalts.

Meanwhile, numerous studies have shown the widespread occurrence of hydrothermal sulfide within both modern oceanic crust (Shanks et al., 1981; Janecky and Seyfried Jr, 1984; Alt et al., 1987, 1989; Alt, 1991, 1995; Alt et al., 2007; Rouxel et al., 2008; Alt and Shanks, 2011) and ophiolites (Duke and Hutchinson, 1974; Haymon et al., 1984, 1989; Alt, 1994; Oeser et al., 2012). On the one hand, low-temperature hydrothermal sulfides have been reported to have ^{34}S < 0‰ (e.g. Alt 1995; Alt and Shanks, 2011; Rouxel et al., 2008; Ono et al., 2012) but are typically formed under T < 200ºC, i.e. away from the locations of magmatic activities, and are associated to low S-content in the rock scale (<0.2%, e.g. Alt and Shanks 2011). They hence do not represent a likely contaminant for MORB and are excluded from the following discussion. On the other hand, massive sulfides originate from efficient seawater sulfate reduction at temperature above 300 °C (Shanks et al., 1981) and are very heterogeneously distributed, according to the hydrothermal plumbing system (Janecky and Seyfried Jr, 1984). Significant contribution of seawater sulfate (having a ^{34}S of +21‰, Rees et al., 1978) leads high-T hydrothermal sulfides to have systematically positive ^{34}S, typically between +2 and +10‰ (e.g. Alt et al., 2007; Peters et al., 2010). Such massive sulfide can thus act as contaminant of erupted melts, hence modifying their S isotope composition.

Massive sulfide and Cl-rich hydrothermal brines assimilation would lead the basalts to both higher Cl/K and increasing ^{34}S relative abundance, but not to higher S-contents owing to sulfide saturation (section 5.2). It is worth noting that because sulfide segregation scales with magmatic differentiation together with crustal contamination, assimilation of hydrothermal sulfides could likely generate the weak trend observed between ^{34}S and proxies of immiscible sulfide fractionation (Fig. 7).

Figure 8 presents ^{34}S co-variation with Cl/K ratios and illustrates two populations of data: a first subset of samples (n=10) exhibits increasing ^{34}S for increasing Cl/K ratios. For these samples, chlorine contamination would have been accompanied by sulfur assimilation, the high ^{34}S of the contaminant being consistent with a high-T hydrothermal origin. The second subset of samples (n=28) does not exhibit any systematic ^{34}S variation with respect to Cl/K. Importantly,

17

the Cl/K range in both subsets of samples is comparable (between 0.06 and 0.5 for most samples, Fig. 8). In other words, both group of samples experienced comparable amount of Cl-contamination, but only the former would be associated to a significant modification of its S isotopic composition, probably reflecting either that hydrothermal sulfides are generated in a temperature range distinct from the one of hyper-saline brines (Shanks et al., 1981; Kelley and Delaney, 1987), or the heterogeneous distribution of massive sulfide in the altered oceanic crust (Alt 1995) that have no reason to be systematically associated with chlorine-contaminants. Considering the natural ^{34}S variability of hydrothermal sulfide, it is difficult to elaborate an accurate mixing model. Two mixing models (I and II) were performed in which two extreme contaminants in $^{34}S/^{32}S$ are chosen (parameters summarized in Table 5). Wall rocks I and II are taken as two realistic contaminants, containing 1 and 3 wt% S and a ^{34}S of +5 and +10‰, respectively (Alt, 1995), and a mean δ^{33}S of +0.018±0.008‰ (1) from Ono et al. (2012), in the range of values also reported by Ono et al. (2007), Rouxel et al. (2008), Peters et al. (2010), and Oeser et al. (2012). As far as we know, no δ^{36}S data are currently reported in the literature for hydrothermal sulfides. Assuming that δ^{36}S = -6.9 × δ^{33}S (Ono et al. 2006; Farquhar et al., 2007), δ^{36}S for hydrothermal sulfides is taken as -0.126‰. MORB endmember is taken as ^{34}S = -1.00‰, δ^{33}S = +0.010‰ and δ^{36}S = -0.071‰ (this study). Maximum contributions required to account for the highest ^{34}S reported in this study range from 3.5 to 0.5% of assimilated wall rock for case I and II, respectively. Such a ^{34}S increase, triggered by hydrothermal sulfide assimilation, does not impact either δ^{33}S or δ^{36}S remaining within our analytical uncertainties (not shown).

Positive deviations of ^{34}S with respect to their isotope baseline (Fig. 4 A) can therefore be accounted for by hydrothermal sulfide assimilation. Discrete contamination processes also better explain the 'spike-like' ^{34}S deviations with respect to the geographic isotope baseline (Fig. 4 A). This explanation does not any longer require the occurrence of a $^{34}S/^{32}S$ isotope fractionation during sulfide exsolution, in agreement with Mandeville et al., (1998;2009) and Labidi et al. (2013). As a corollary, the subset of samples that do not show any systematic trend between ^{34}S and Cl/K can be considered as uncontaminated from the S isotope prospective, hence representing MORB mantle source $^{33\text{-}34\text{-}36}S$ values. Uncontaminated

18

samples have a mean ^{34}S of -0.89±0.11‰ with values ranging between -1.12 and -0.70‰.

7. Addressing the marble-cake model from a S isotope perspective

Although radiogenic and noble gases isotope ratios of the studied samples lie within the depleted MORB spectrum defined in Workman and Hart (2005) and Moreira et al. (1998), their isotope variability highlights subtle source heterogeneity, consistent with the marble-cake assemblage model (Allègre and Turcotte, 1986; Hamelin et al., 2011). In this frame, the depleted endmember (DM) would represent the residual fraction of multiple melt extractions over geological times (Workman and Hart, 2005). This endmember has unradiogenic ^{206}Pb/^{204}Pb (i.e. close to the geochron, ^{206}Pb/^{204}Pb$_{DM}$ = 17.53, Workman and Hart, 2005; Jackson and Carlson 2011) compared to the more radiogenic HIMU endmember (^{206}Pb/^{204}Pb$_{HIMU}$ = 21.19, Jackson and Dasgupta, 2008). Following Hofmann and White (1982), Chauvel et al. (1992, 1995) and Kelley et al. (2005), the HIMU component is interpreted as recycled oceanic crust that lost a significant fraction of its lead (> 75%), generating high U/Pb and time-integrated radiogenic ^{206}Pb/^{204}Pb.

Uncontaminated samples exhibit significant ^{206}Pb/^{204}Pb variability, increasing northward from 18 to 19.5 (Fig. 9), yet ^{34}S variation remains weak: all values range from -1.12±0.02 to -0.72±0.02‰, i.e. a maximal spread of only 0.40‰ (Table 2). Such a moderate ^{34}S variability in the PAR mantle points toward a recycled component that has a modest impact on the bulk sulfur budget. In the detail, however, a second-order ^{34}S/^{32}S variability can be resolved (Fig. 9-B). The 66-56°S segment exhibits homogeneous ^{34}S averaging at -0.90±0.05‰, whereas two sub-zones occur in the 53-41°S segment, separated by a geochemical boundary at 45°85' S (Fig. 9-B), yet without any tectonic discontinuity: between 45°85' S and 53° S, the mean ^{34}S is -0.79±0.04‰ whereas it shifts at -1.02±0.09‰ between 41° S and 45°85' S. The northern domain of the PAR (between 41 and 45°85' S) is the closest to the Foundation hotspot (Fig. 1). The geochemical features of the northern zone are thus susceptible to result from a localized plume-ridge interaction. Maia et al. (2001) however showed that the Foundation hotspot is associated to high ^{206}Pb/^{204}Pb, in disagreement with the values observed in MORB glasses. Furthermore, glasses from the 41-45°85'S section do not display any plume-type ^{4}He/^{3}He ratios

19

(Moreira et al., 2008). Peculiar ^{34}S observed at this ridge section may thus rather reflect isotope heterogeneity of the bulk MORB mantle.

7.1. Mixing endmembers identification

^{34}S variations with respect to ^{206}Pb/^{204}Pb of uncontaminated samples are shown in Fig. 10. In the northern part (45°85' S to 41°S), ^{34}S of the glasses are   -0.20‰ lower than in the two other locations, at a given ^{206}Pb/^{204}Pb. Such trends illustrate that stable isotopes of sulfur can reveal a still-unrecorded type of mantle heterogeneity along ocean ridges. The weak positive trends between ^{34}S and ^{206}Pb/^{204}Pb exhibited by the samples, if any, show that the DM endmember has a broadly lower ^{34}S than HIMU components.

Homogeneous DM associated with a variable S/Pb ratio in the HIMU endmember can account for along-ridge δ^{34}S variations if the HIMU component south of 45°85'S has a higher S/Pb ratio than in the northern area. Introducing HIMU-S and HIMU-N terms to describe South and North of 45°85'S endmembers respectively, an ad-hoc model can be constructed to derive both ^{34}S and S/Pb ratio for DM, HIMU-N and HIMU-S. According to Workman and Hart (2005), the Pb amount in DM is 0.014 ppm. The Pb abundance in HIMU-S and –N is derived from Pb-contents of present-day altered oceanic crust: Kelley et al. (2003) provide an estimate of 0.43 ppm Pb, indistinguishable within uncertainty from previous estimates by Chauvel et al. (1992) and Rehkamper and Hofmann (1997). Between 58 and 98 % of Pb must be lost during slab dehydration to generate the high ^{206}Pb/^{204}Pb with time (Chauvel et al., 1992; Kelley et al., 2005). The Pb abundance in the HIMU component can therefore be roughly estimated between 0.18 and 0.008 ppm. The S amount in DM is taken at 200 ppm (Luguet et al., 2003), the S abundance of altered oceanic crust being 930 ppm (Rouxel et al., 2008; Alt and Shanks, 2011). As Pb in altered oceanic crust is essentially carried by sulfides (Kelley et al., 2003), S abundance in the subduction-processed slab can be roughly estimated, and assuming that $D_{Pb}^{rock\text{-}fluids}$ is broadly equal to $D_{S}^{rock\text{-}fluids}$, S abundance of the HIMU mantle endmember must range between 385 and 18 ppm. It is noted that such first-order values are derived here for estimation purposes only, and that future studies are needed to refine estimations of S

20

abundance in recycled oceanic crust.

Using these parameters, ^{34}S for both DM and HIMU of -1.40±0.50 and +3.00±1.00‰ respectively, can be derived together with S abundances in recycled endmembers of 300±50 ppm and 175±50 ppm for HIMU-S and HIMU-N, respectively (Table 6). Inferred S mantle source abundance is moderate, ranging between 200 and 220 ppm, remaining within the uncertainty of the MORB mantle estimate (Luguet et al., 2003). Additionally, the S abundance in HIMU component(s) drops only by a factor of 2 across the 45°85'S boundary. The proportion of recycled oceanic crust in the MORB mantle source derived from the proposed model is 10±5%, value consistent with the Sobolev et al. (2007) independent estimate.

The off-axis samples PAC2 DR42-1c and PAC2 DR39-4 have ^{34}S values of -1.57±0.11‰ and -1.25±0.12‰. As mentioned earlier, off-axis lavas may record more accurately the heterogeneity of the mantle than on-axis samples: such ^{34}S values would be accounted for by a HIMU component that would be locally severely S-depleted (i.e. 30 ppm S), located north of 45°85'S (Fig. 10). Its ^{34}S hence better reflects the DM composition, in agreement within uncertainty with the above estimate.

7.2. An independent constraint on the age of recycled oceanic crust?

Since Hofmann and White (1982), the age of the HIMU component is considered as broadly Proterozoic, typically being 1.8 Ga old. However, olivine-hosted sulfide from Mangaia Island (the most extreme HIMU-type plume, see Willbold and Stracke, 2006; Jackson and Dasgupta, 2008) have highly variable yet non-zero •^{33}S values, down to -0.4‰ (Cabral et al., 2013). Such values only occur in the Archean rock record (Farquhar et al., 2000), bringing new constraints on HIMU age, typically > 2.4 Ga.

For the PAR basalts, however, even for samples with the highest ^{206}Pb/^{204}Pb, •^{33}S values remain within uncertainty of CDT. The lack of trend between ^{34}S and •^{33}S tightly constrains •^{33}S for the HIMU component(s) in the PAR mantle to lie between +0.050 and -0.050‰, and is inconsistent with a value <-0.3‰ (Fig. 11). Our •^{36}S estimate for HIMU falls between +0.350 and -0.350‰ (not shown). Our positive ^{34}S estimate for HIMU also differs from the Cabral et al. (2013) value (< -7‰). Positive ^{34}S with near-zero Δ^{3}S (and •^{36}S) of the HIMU component(s) in the PAR

21

mantle can be reconciled with the Mangaia estimate considering heterogeneous recycled oceanic crust from the S isotope perspective.

If Archean in age, the recycled oceanic crust in the PAR mantle could have incorporated either minor amounts of Archean atmospheric sulfur, and/or that such component carries Archean sulfur in which positive and negative $\bullet^{33}$S pools are mixed together in original proportions (i.e. $\bullet^{33}$S ~0‰).

Alternatively, our mass-dependent ^{33}S abundance estimate for HIMU in the PAR mantle is consistent with a post-Archean age, requiring an age-heterogeneity for this mantle component. Such a conclusion is consistent with a HIMU model-age likely reflecting a mixing between older (archean) and younger (Proterozoic to Phanerozoic) components as previously suggested (Allègre, 1982; Halliday et al., 1992; Schilling et al., 1992; Hofmann, 1997; Thirlwall, 1997; Dosso et al., 1999).

8. Significance of a non-chondritic ^{34}S for the MORB mantle

Our data further emphasize that the depleted mantle is characterized by low ^{34}S compared to chondrites. The proposed ^{34}S estimate here of -1.40±0.50‰ is statistically indistinguishable from the South-Atlantic depleted-mantle (^{34}S =-1.28±0.33‰, Labidi et al., 2013), but extends such finding to the large mantle-domain studied here. Importantly, it is shown that recycled oceanic crust being pervasively occurring in the mantle carries a relatively high ^{34}S, and hence cannot explain the sub-chondritic ^{34}S value recorded by MORB worldwide.

The depleted endmember hosts endogenous sulfur (as opposed to recycled components) and because partial melting may preserve the ^{34}S/^{32}S ratio of lavas and residues (see section 6), such sub-chondritic values have been inherited from the primitive mantle. In the following section, we provide a detailed discussion on such non-chondritic ^{34}S/^{32}S ratio for the Earth's mantle.

8.1 Mantle-crust complementarity: a view from S isotopes

Assuming that the bulk Earth has a chondritic ^{34}S, a non-chondritic composition for the mantle must be balanced by another reservoir. Our ^{34}S estimate for the recycled oceanic crust is

22

~3.00‰ with a S-content lower than 300 ppm, compared to ~200 ppm S for the depleted mantle (section 7.1). Here, we suggest here that occurrence of such recycled component increases the accessible mantle ^{34}S from -1.4±0.5‰ (pure DM value) to the observed value of +0.89±0.11‰ (section 6.2). It could be speculated that an inaccessible fraction of the mantle (i.e. the lower mantle) is constituted by higher proportions of recycled oceanic crust, hence leading to an overall chondritic ^{34}S/^{32}S of the silicate Earth. However, unless more than 40% of the lower mantle is constituted of recycled oceanic crust, such model does not lead to an overall chondritic ^{34}S value, hence failing to account for the observation.

Non-subducted continental sulfur, likely brought to the surface by partial melting of the primitive mantle, could be the complementary reservoir. Surface reservoirs include continents, oceans, and altered oceanic crust (see table 7 for details). Our data compilation from the literature lead to a mean surficial reservoir containing 750 ppm S with a mean ^{34}S of   +1.0‰ (Rees, 1978; Rouxel et al., 2008; Alt and Shanks, 2011; Alt, 1995; Wedepohl, 1995). Uncertainties and likely sampling biases associated to the cited studies are such that the ^{34}S of the surface reservoir is estimated with a ±3‰ uncertainty. As a first order, the exogenous sulfur seems therefore indistinguishable from the upper mantle estimate derived here. For the mantle, we use the mean MORB mantle value derived in this study (^{34}S of -0.89±0.11‰) rather than the DM estimate in order to implicitly take into account the occurrence of recycled oceanic crust in the upper mantle.

In a Sm/Nd chondritic Earth model, the ^{147}Sm–^{143}Nd systematics of terrestrial reservoirs requires the depleted mantle to be ~25% of the bulk mantle (DePaolo, 1980), requiring surface sulfur to have a ^{34}S of +8±2‰ to balance the negative value of the MORB mantle around to chondritic value (Table 7). It is worth noting that the disequilibrium is more pronounced in a non-chondritic Earth model, where the depleted mantle corresponds to 80% of the bulk mantle (Caro and Bourdon, 2010), a size that has been independently substantiated by data on diamonds from the lower mantle (see Palot et al., 2012): in such a model, surface sulfur must have a ^{34}S of +25±6‰. These values are inconsistent with the current estimates of surface reservoirs inventory. Unless the current estimates of surficial reservoirs are wrong by more

23

than one order of magnitude in terms of S abundance and/or ^{34}S, it can be concluded that the bulk silicate Earth is non-chondritic in terms of ^{34}S/^{32}S.

8.2 ^{34}S/^{32}S fractionation during magma ocean stage?

The lithospheric mantle exhibit only subtle deviations from chondritic relative abundances of S, Se and Te (Lorand et al., 2003; Konig et al., 2012;2014). Although (S/Ir)$_N$ ratios are 0.65 (e.g. Becker et al., 2006) i.e. clearly of non CI-type, several authors have argued that mantle S, Se and Te budgets could be accounted for by a late accretionary component with highly siderophile elements (e.g. McDonough and Sun, 1995; Rose-Weston et al., 2009; Lorand and Alard, 2010). Both McDonough and Sun (1995) and Wang and Becker (2013) proposed the late-accreted component to be slightly volatile-depleted, i.e. with low (S/Ir)$_N$ ratio, explaining the mantle value.

Alternatively, late-accreted S can be assumed to be partially lost from the magma ocean to the outer space by degassing and/or evaporation, as dictated by its low condensation temperature (~ 700 K under canonical nebular conditions, Lodders, 2003). Such a process could affect the ^{34}S of the mantle, possibly accounting for the observed shift between the present-day MORB mantle and chondrites, also explaining the sub-chondritic (S/Ir)$_N$ ratios.

According to kinetic theory of gases, an isotope fractionation during evaporation of elemental sulfur can be described as follows:

$$a_{evaporation} = \sqrt{32/34} = 0.9701 \ (17)$$

The $_{evaporation}$ value for ^{56}Fe^{32}S and ^{56}Fe^{34}S evaporation becomes 0.9888. In other words, the evaporated sulfur-species are strongly enriched in ^{32}S with respect to the residue (by 30‰ for S evaporation and by 11‰ for FeS evaporation), a process that would lead to a ^{34}S increase of planetary mantles. Positive ^{34}S-values of lunar soils (up to +18‰, Ding et al., 1983) have been explained by such process. The Earth's mantle ^{34}S is however lower than in chondrites, in contrast to the higher values expected from evaporation.

Sulfur could be partitioned between vapor and melt in a similar manner to what is observed in

24

present-day sub-aerial volcanism (Wallace and Edmonds, 2011). According to the data compilation of Mandeville et al. (2009), degassed SO_2 would exhibit a 2‰ ^{34}S enrichment with respect to reduced sulfur in the melt at 1200°C, reflecting isotope equilibrium degassing. In that case, 70 and 50% of sulfur must be degassed (and lost to the outer space) as SO_2 in closed and open systems respectively, to account for the negative ^{34}S observed in the present-day mantle.

Se is however known to be highly refractory with respect to magmatic degassing (Jenner et al., 2012). Such sulfur degassing would severely decrease the S/Se ratio of the mantle to sub-chondritic values, in contrast with its slightly super-chondritic value observed in the lithospheric mantle (by ~30±15%, Lorand et al., 2003; Lorand and Alard, 2010).

8.3. A core-mantle differentiation record and its implications

Our new data further support that non-chondritic $^{34}S/^{32}S$ of the mantle results from core-mantle differentiation. Sulfur being siderophile (Li and Agee, 2001; Rose-Weston et al., 2009), the terrestrial core is potentially able to complement the mantle. Furthermore, simple mass balance requires the core to carry more than 97% of the bulk-Earth sulfur (Dreibus and Palme, 1996). In this context, if the primitive mantle (i.e. that equilibrated with the core) has a $^{34}S/^{32}S$ ratio equal to the present-day depleted mantle (consistent with a lack of S isotope fractionation during partial melting) and assuming a chondritic bulk-Earth, the inferred $_{core-mantle}$ would be 1.00140 or 1.00040 depending if the S incorporation in the core occurs under closed or open system, respectively (Labidi et al., 2013). In both cases, the ^{34}S of the terrestrial core is expected to be +0.07‰, very close to the chondritic value, as this reservoir would contain most of the terrestrial sulfur (Labidi et al., 2013). If enstatite chondrites are considered as the most likely parent bodies of the Earth (Javoy 1995, and Javoy et al., 2010), having a mean ^{34}S of -0.26±0.07‰, (Gao and Thiemens, 1993b), the $_{core-mantle}$ decreases to 1.00110 and 1.00025 for closed and open system, respectively.

As reduction/oxidation processes drive all the $^{34}S/^{32}S$ fractionations at high temperature, the required metal-silicate fractionation in this study implies that sulfur in the metal is under a more oxidized form than in the mantle (Taylor, 1986; Ohmoto and Goldhaber, 1997). This can match

25

observation if sulfur dissolves in the metal under its metallic form (S^0, compared to S^{2-} in the residual silicate mantle), but such an inference remains to be demonstrated. In all cases, the $^{34}S/^{32}S$ record of core-mantle equilibrium implies that sulfur and elements of comparable volatilities such as zinc, fluorine or lead were provided at least partly before the late-accretion event, and is therefore incompatible with models suggesting that the mantle was deprived of volatiles (including lead) before the late stage accretion (e.g. Albarède, 2009).

Sulfur, selenium and tellurium have similar condensation temperature in canonical nebular conditions, of 700 K (Lodders, 2003). As these elements have distinct metal-silicate partition coefficient (Rose-Weston et al., 2009), chondritic Se/Te would probe a mantle budget for these two elements being dominated by late-accreted components (Wang and Becker 2013). However, chondritic Se/Te ratios of the mantle are based on the analysis of lithospheric peridotites that are overprinted by metasomatism, so that their Se/Te ratio may not be representative of bulk silicate Earth (Koenig et al., 2014). If chondritic relative abundances of Se and Te were still considered to reflect asthenospheric mantle composition (Wang and Becker 2013), hybrid models are required to reconcile near-chondritic Se/Te (Lorand and Alard 2010, Wang and Becker 2013) with non-chondritic $^{34}S/^{32}S$ of the mantle. In such models, mantle sulfur must be seen as a mixing between a fractionated leftover (with even lower $^{34}S/^{32}S$) and a chondritic late-accreted component (with chondritic $^{34}S/^{32}S$), implying the metal-silicate fractionation of S isotopes to be even higher than determined above. Assuming more than 90% of Se and Te is provided via late-accretion (Wang and Becker 2013), and that an unconstrained proportion of S results from a core-mantle equilibrium leftover, a super chondritic S/Se (and S/Te) for the mantle is expected. The S/Se ratio of fertile lherzolites is actually super-chondritic by 30±15% (Lorand and Alard, 2010). Consequently, although Lorand and Alard (2010) proposed that petrogenetic processes occurring in the lithospheric mantle account for such super-chondritic S/Se ratio, a hybrid model for S and Se origin could also constitute a viable explanation, resulting from the mixing of a highly S/Se fractionated mantle (i.e. leftover from a core-mantle segregation) with a chondritic component. If correct, the proportion of late-accreted sulfur reaches 70±15‰, and the core-mantle $^{34}S/^{32}S$ isotope fraction

26

would be predicted to be 1.00235±0.00025 or 1.00068±0.00007 for batch equilibrium and open system fractionation, respectively.

9. Conclusion

Pacific-Antarctic ridge basalts are all FeS-saturated. Two independent quantification of sulfide fractionation, based on S and Cu abundance systematics, yield indistinguishable estimates of lost immiscible sulfide in bulk precipitated minerals of 0.19±0.07% and 0.19±0.04% respectively.

$•^{33}$S and $•^{36}$S of the PAR basalts are both homogeneous and indistinguishable from the CDT international standard, whereas ^{34}S are significantly heterogeneous. Their first-order $^{34}S/^{32}S$ variability is hardly explained by a sulfide-silicate $^{34}S/^{32}S$ fractionation but can instead be accounted for by hydrothermal sulfide assimilation. This is supported by evidence that almost all of the on-axis PAR basalts have assimilated Cl-rich brines, as usual in fast-spreading ridge context. Data point to an average ^{34}S of -0.89±0.11 ‰ for uncontaminated samples, distinct from the chondritic estimate of +0.04±0.31‰ (Gao and Thiemens, 1993a,b). The sub-chondritic $^{34}S/^{32}S$ ratio therefore extends to the Pacific-Antarctic domain the observation previously made on south-Atlantic basalts.

Weak trends between ^{34}S and $^{206}Pb/^{204}Pb$ in uncontaminated samples indicate that the recycled component has a modest impact on the mean ^{34}S of the MORB mantle, but in detail, extrapolation of these trends yields estimates of ^{34}S for depleted mantle and HIMU endmembers of -1.40±0.50 and +3.00±1.00 ‰, respectively. As a corollary, these estimates imply that the oceanic crust recycled in the Earth's mantle cannot be responsible for the MORB negative ^{34}S with respect to chondrites. The negative ^{34}S of the terrestrial mantle cannot be balanced by the ^{34}S of the surficial reservoirs. The terrestrial core may contain more than 95% of the Earth's sulfur such that a metal-silicate isotope fractionation may easily lead to a residual silicate mantle with a $^{34}S/^{32}S$ distinct from chondrites. Such a record of the core-mantle differentiation has critical implications for the timing of incorporation of moderately volatile elements to the Earth, especially implying a delivery occurring before late-accretion events.

27

11. Acknowledgments

References

Albarède, F., 2009. Volatile accretion history of the terrestrial planets and dynamic implications. Nature 461 (7268), 1227–1233.

Allègre, C., 1982. Chemical geodynamics. Tectonophysics 81 (3), 109–132.

Allègre, C., Turcotte, D., 1986. Implications of a two-component marble-cake mantle. Nature 323 (6084), 123–127.

Alt, J., 1991. The mineralogy and isotopic composition of sulfur in Layer 3 gabbros from the Indian Ocean, ODP Hole 735B. In: Proc. OOP, Sci. Results. Vol. 118. College Station, TX (Ocean Drilling Program), pp. 113–125.

Alt, J., 1994. A sulfur isotopic profile through the Troodos ophiolite, Cyprus: primary compo- sition and the effects of seawater hydrothermal alteration. Geochimica et cosmochimica acta 58 (7), 1825–1840.

Alt, J., 1995. Sulfur isotopic profile through the oceanic crust: Sulfur mobility and seawater- crustal sulfur exchange during hydrothermal alteration. Geology 23 (7), 585–588.

Alt, J., Anderson, T., Bonnell, L., 1989. The geochemistry of sulfur in a 1.3 km section of hydrothermally altered oceanic crust, DSDP Hole 504B. Geochimica et Cosmochimica Acta 53 (5), 1011–1023.

Alt, J., Lonsdale, P., Haymon, R., Muehlenbachs, K., 1987. Hydrothermal sulfide and oxide deposits on seamounts near 21°N, East Pacific Rise. Geological Society of America Bulletin 98 (2), 157–168.

Alt, J., Shanks, W., 2011. Microbial sulfate reduction and the sulfur budget for a complete section of altered oceanic basalts, IODP Hole 1256D (eastern Pacific). Earth and Planetary Science Letters 310 (1-2), 73–83.

Alt, J., Shanks III, W., Bach, W., Paulick, H., Garrido, C., Beaudoin, G., 2007. Hydrothermal alteration and microbial sulfate reduction in peridotite and gabbro exposed by detachment faulting at the Mid-Atlantic Ridge, 15°20 N (ODP Leg 209): A sulfur and oxygen isotope study. Geochemistry Geophysics Geosystems 8 (8), Q08002.

Arevalo, R., McDonough, W., 2010. Chemical variations and regional diversity observed in MORB. Chemical Geology 271 (1-2), 70–85.

Backnaes, L., Deubener, J., 2011. Experimental studies on sulfur solubility in silicate melts at near-atmospheric pressure. Reviews in Mineralogy and Geochemistry 73 (1), 143–165.

Batiza, R., Vanko, D., 1984. Petrology of young Pacific seamounts. Journal of Geophysical Research 89 (B13), 11235–11.

Becker, H., Horan, M., Walker, R., Gao, S., Lorand, J., Rudnick, R., 2006. Highly siderophile element composition of the Earth's primitive upper mantle: Constraints from new data on peridotite massifs and xenoliths. Geochimica et Cosmochimica Acta 70 (17), 4528–4550.

Bézos, A., Humler, E., 2005. The Fe3+/ Fe ratios of MORB glasses and their implications for mantle melting. Geochimica et cosmochimica acta 69 (3), 711–725.

Bézos, A., Lorand, J., Humler, E., Gros, M., 2005. Platinum-group element systematics in Mid- Oceanic Ridge basaltic glasses from the Pacific, Atlantic, and Indian Oceans. Geochimica et Cosmochimica Acta 69 (10), 2613–2627.

Bigeleisen, J., Mayer, M., 1947. Calculation of equilibrium constants for isotopic exchange reactions. The Journal of Chemical Physics 15, 261.

Birch, F., 1964. Density and composition of mantle and core. Journal of geophysical research 69 (20), 4377–4388.

Bonifacie, M., Jendrzejewski, N., Agrinier, P., Humler, E., Coleman, M., Javoy, M., 2008. The chlorine isotope composition of Earth's mantle. Science 319 (5869), 1518–1520.

Brandl, P., Beier, C., Regelous, M., Abouchami, W., Haase, K., Garbe-Schonberg, D., Galer, S., 2012. Volcanism on the flanks of the East Pacific Rise: Quantitative constraints on mantle heterogeneity and melting processes. Chemical Geology.

298, 41-56

Briais, A., Ondréas, H., Klingelhoefer, F., Dosso, L., Hamelin, C., Guillou, H., et al., 2009. Origin of volcanism on the flanks of the Pacific-Antarctic ridge between 41°30 S and 52 S. Geochem. Geophys. Geosyst 10, Q09001.

Cabral, R. A., Jackson, M. G., Rose-Koga, E. F., Koga, K. T., Whitehouse, M. J., Antonelli, M. A., ... & Hauri, E. H. (2013). Anomalous sulphur isotopes in plume lavas reveal deep mantle storage of Archaean crust. *Nature*, *496*(7446), 490-493.

Caro, G., Bourdon, B., 2010. Non-chondritic Sm/Nd ratio in the terrestrial planets: Consequences for the geochemical evolution of the mantle–crust system. Geochimica et Cosmochimica Acta 74 (11), 3333–3349.

Carroll, M., Webster, J., 1994. Solubilities of sulfur, noble gases, nitrogen, chlorine, and fluorine in magmas. Reviews in Mineralogy and Geochemistry 30 (1), 231–279.

Chaussidon, M., Albarede, F., Sheppard, S., 1989. Sulphur isotope variations in the mantle from ion microprobe analyses of micro-sulphide inclusions. Earth and Planetary Science Letters 92 (2), 144–156.

Chaussidon, M., Sheppard, S., Michard, A., 1991. Hydrogen, sulphur and neodymium isotope variations in the mantle beneath the EPR at 12°50'N. Stable Isotope Geochemistry: a Tribute to Salmuel Epstein. Geochemical Society, Special Publication 3, 325–337.

Chauvel, C., Goldstein, S., Hofmann, A., 1995. Hydration and dehydration of oceanic crust controls Pb evolution in the mantle. Chemical Geology 126 (1), 65–75.

Chauvel, C., Hofmann, A., Vidal, P., 1992. HIMU–EM: the French Polynesian connection. Earth and Planetary Science Letters 110 (1-4), 99–119.

Christie, D., Carmichael, I., Langmuir, C., 1986. Oxidation states of mid-ocean ridge basalt glasses. Earth and Planetary Science Letters 79 (3-4), 397–411.

Clog, M., Aubaud, C. Cartigny, P., Dosso, L. 2013. The hydrogen isotopic composition and water content of southern Pacific MORB: A reassessment of the D/H ratio of the depleted mantle reservoir. Earth and Planetary Science Letters 381, 156-165

Cottrell, E., Kelley, K., 2011. The oxidation state of Fe in MORB glasses and the oxygen fugacity of the upper mantle. Earth and Planetary Science Letters 305 (3-4), 270–282.

Czamanske, G., Moore, J., 1977. Composition and phase chemistry of sulfide globules in basalt from the Mid-Atlantic Ridge rift valley near 37° N. Bulletin of the Geological Society of America 88 (4), 587.

DeMets, C., Gordon, R., Argus, D., Stein, S., 1990. Current plate motions. Geophysical journal international 101 (2), 425–478.

DePaolo, D., 1980. Crustal growth and mantle evolution: inferences from models of element transport and Nd and Sr isotopes. Geochimica et Cosmochimica Acta 44 (8), 1185–1196.

Ding, T., Thode, H., Rees, C., 1983. Sulphur content and sulphur isotope composition of orange and black glasses in apollo 17 drive tube 74002/1. Geochimica et Cosmochimica Acta 47 (3), 491–496.

Dosso, L., Bougault, H., Langmuir, C., Bollinger, C., Bonnier, O., Etoubleau, J., 1999. The age and distribution of mantle heterogeneity along the Mid-Atlantic Ridge (31–41°N). Earth and planetary science letters 170 (3), 269–286.

Dreibus, G., Palme, H., 1996. Cosmochemical constraints on the sulfur content in the Earth's core. Geochimica et Cosmochimica Acta 60 (7), 1125–1130.

Duke, N., Hutchinson, R., 1974. Geological relationships between massive sulfide bodies and ophiolitic volcanic rocks near York Harbour, Newfoundland. Canadian Journal of Earth Sciences 11 (1), 53–69.

Farquhar, J., Bao, H., Thiemens, M., 2000. Atmospheric influence of Earth's earliest sulfur cycle. Science 289 (5480), 756.

Farquhar, J., Johnston, D., Boswell, W. 2007 Implications of conservation of mass effects on mass-dependent isotope fractionations: Influence of network structure on sulfur isotope phase space of dissimilatory sulfate reduction. Geochimica et Cosmochimica Acta (71) 5862–5875

Farquhar, J., Wing, B., 2003. Multiple sulfur isotopes and the evolution of the atmosphere. Earth and Planetary Science Letters 213 (1-2), 1–13.

Francis, R., 1990. Sulfide globules in mid-ocean ridge basalts (MORB), and the effect of oxygen abundance in Fe–S–O liquids on the ability of those liquids to partition metals from MORB and komatiite magmas. Chemical Geology 85 (3-4), 199–213.

Gaetani, G., Grove, T., 1997. Partitioning of moderately siderophile elements among olivine, silicate melt, and sulfide melt: Constraints on core formation in the Earth and Mars. Geochimica et Cosmochimica Acta 61 (9), 1829–1846.

Gaillard, F., Scaillet, B., 2009. The sulfur content of volcanic gases on Mars. Earth and Planetary Science Letters 279 (1-2),

29

34–43.

Gao, X., Thiemens, M., 1993a. Isotopic composition and concentration of sulfur in carbonaceous chondrites. Geochimica et Cosmochimica Acta 57 (13), 3159–3169.

Gao, X., Thiemens, M., 1993b. Variations of the isotopic composition of sulfur in enstatite and ordinary chondrites. Geochimica et Cosmochimica Acta 57 (13), 3171–3176.

Géli, L., Bougault, H., Aslanian, D., Briais, A., Dosso, L., Etoubleau, J., Le Formal, J., Maia, M., Ondréas, H., Olivet, J., et al., 1997. Evolution of the Pacific–Antarctic Ridge south of the Udintsev fracture zone. Science 278 (5341), 1281.

Halliday, A. N., Davies, G. R., Lee, D.-C., Tommasini, S., Paslick, C. R., Fitton, J., James, D. E., 1992. Lead isotope evidence for young trace element enrichment in the oceanic upper mantle. Nature 359, 623–627.

Hamelin, C., Dosso, L., Hanan, B., Barrat, J., Ondréas, H., et al., 2010. Sr-Nd-Hf isotopes along the Pacific Antarctic Ridge from 41 to 53° S. Geophysical Research Letters 37, L10303.

Hamelin, C., Dosso, L., Hanan, B., Moreira, M., Kositsky, A., Thomas, M., 2011. Geochem- ical portray of the Pacific Ridge: New isotopic data and statistical techniques. Earth and Planetary Science Letters 302 (1), 154–162.

Harvey, J., Gannoun, A., Burton, K., Rogers, N., Alard, O., Parkinson, I., 2006. Ancient melt extraction from the oceanic upper mantle revealed by Re–Os isotopes in abyssal peridotites from the Mid-Atlantic ridge. Earth and Planetary Science Letters 244 (3), 606–621.

Haymon, R., Koski, R., Abrams, M., 1989. Hydrothermal discharge zones beneath massive sulfide deposits mapped in the Oman ophiolite. Geology 17 (6), 531–535.

Haymon, R., Koski, R., Sinclair, C., 1984. Fossils of hydrothermal vent worms from Cretaceous sulfide ores of the Samail Ophiolite, Oman. Science 223 (4643), 1407–1409.

Hofmann, A., 1997. Mantle geochemistry: the message from oceanic volcanism. Nature 385 (6613), 219–229.

Hofmann, A., White, W., 1982. Mantle plumes from ancient oceanic crust. Earth and Planetary Science Letters 57 (2), 421–436.

Holzheid, A., Grove, T., 2002. Sulfur saturation limits in silicate melts and their implications for core formation scenarios for terrestrial planets. American Mineralogist 87 (2-3), 227–237.

Jackson, M., Dasgupta, R., 2008. Compositions of HIMU, EM1, and EM2 from global trends between radiogenic isotopes and major elements in ocean island basalts. Earth and Planetary Science Letters 276 (1-2), 175–186.

Jackson, M. G., & Carlson, R. W. 2011. An ancient recipe for flood-basalt genesis. *Nature*, *476*(7360), 316-319.

Janecky, D., Seyfried Jr, W., 1984. Formation of massive sulfide deposits on oceanic ridge crests: incremental reaction models for mixing between hydrothermal solutions and seawater. Geochimica et Cosmochimica Acta 48 (12), 2723–2738.

Javoy, M., 1995. The integral enstatite chondrite model of the Earth. Geophysical Research Letters 22 (16), 2219–2222.

Javoy, M., Kaminski, E., Guyot, F., Andrault, D., Sanloup, C., Moreira, M., Labrosse, S., Jambon, A., Agrinier, P., Davaille, A., Jaupart, C., 2010. The chemical composition of the Earth: Enstatite chondrite models. Earth and Planetary Science Letters 293 (3), 259–268.

Jenner, F., Arculus, R., Mavrogenes, J., Dyriw, N., Nebel, O., Hauri, E., 2012. Chalcophile element systematics in volcanic glasses from the northwestern Lau Basin. Geochemistry Geo- physics Geosystems 13 (null), Q06014.

Jenner, F., O'Neill, H., Arculus, R., Mavrogenes, J., 2010. The magnetite crisis in the evolution of arc-related magmas and the initial concentration of au, ag and cu. Journal of Petrology 51 (12), 2445–2464.

Jugo, P., Wilke, M., Botcharnikov, R., 2010. Sulfur K-edge XANES analysis of natural and synthetic basaltic glasses: Implications for S speciation and S content as function of oxygen fugacity. Geochimica et Cosmochimica Acta 74 (20), 5926–5938.

Kanehira, K., Yui, S., Sakai, H., Sasaki, A., 1973. Sulphide globules and sulphur isotope ratios in the abyssal tholeiite from the Mid-Atlantic Ridge near 30 N latitude. Geochem. J 7, 89–96.

Keays, R., 1995. The role of komatiitic and picritic magmatism and S-saturation in the formation of ore deposits. Lithos 34 (1-3), 1–18.

Kelley, D., Delaney, J., 1987. Two-phase separation and fracturing in mid-ocean ridge gabbros at temperatures greater than 700 °C. Earth and planetary science letters 83 (1-4), 53–66.

Kelley, K., Cottrell, E., 2012. The influence of magmatic differentiation on the oxidation state of Fe in a basaltic arc magma. Earth and Planetary Science Letters 329, 109–121.

Kelley, K., Plank, T., Farr, L., Ludden, J., Staudigel, H., 2005. Subduction cycling of U, Th, and Pb. Earth and Planetary

Science Letters 234 (3), 369–383.

Kelley, K., Plank, T., Ludden, J., Staudigel, H., 2003. Composition of altered oceanic crust at ODP Sites 801 and 1149. Geochem. Geophys. Geosyst 4 (6), 8910.

Klingelhoefer, F., Ondréas, H., Briais, A., Hamelin, C., Dosso, L., et al., 2006. New structural and geochemical observations from the pacific-antarctic ridge between 52° 45 S and 41° 15 S. Geophysical research letters 33, L21312.

Konig, S., Luguet, A., Lorand, J., Wombacher, F., Lissner, M., 2012. Selenium and tellurium systematics of the Earth's mantle from high precision analyses of ultra-depleted orogenic peridotites. Geochimica et Cosmochimica Acta 86, 354–366.

König, S., Lorand, J. P., Luguet, A., & Graham Pearson, D. 2014. A non-primitive origin of near-chondritic S–Se–Te ratios in mantle peridotites; implications for the Earth•s late accretionary history. *Earth and Planetary Science Letters*, *385*, 110-121.

Labidi, J., Cartigny, P., Birck, J., Assayag, N., Bourrand, J., 2012. Determination of multiple sulfur isotopes in glasses : a reappraisal of the MORB $\delta^{34}S$. Chemical Geology 334, 189–198.

Labidi, J., Cartigny, P., Moreira, M. 2013 Non-chondritic sulphur isotope composition of the terrestrial mantle. Nature, 501, 208-211

Le Roux, P., Le Roex, A., Schilling, J., Shimizu, N., Perkins, W., Pearce, N., 2002. Mantle heterogeneity beneath the southern Mid-Atlantic Ridge: trace element evidence for contamination of ambient asthenospheric mantle. Earth and Planetary Science Letters 203 (1), 479–498.

Le Roux, P., Shirey, S., Hauri, E., Perfit, M., Bender, J., 2006. The effects of variable sources, processes and contaminants on the composition of northern EPR MORB (8–10° N and 12– 14° N): Evidence from volatiles (H2O, CO2, S) and halogens (F, Cl). Earth and Planetary Science Letters 251 (3), 209–231.

Lee, C.-T. A., Luffi, P., Chin, E. J., Bouchet, R., Dasgupta, R., Morton, D. M., Le Roux, V., Yin, Q.-z., Jin, D., 2012. Copper systematics in arc magmas and implications for crust-mantle differentiation. Science 336 (6077), 64–68.

Li, J., Agee, C., 2001. Element partitioning constraints on the light element composition of the Earth's core. Geophys. Res. Lett 28 (1), 81–84.

Lorand, J., 1987. Cu–Fe–Ni–S mineral assemblages in upper-mantle peridotites from the Table Mountain and Blow-Me-Down Mountain ophiolite massifs (Bay of Islands area, Newfoundland): Their relationships with fluids and silicate melts. Lithos 20 (1), 59–76.

Lorand, J., 1988. Fe–Ni–Cu sulfides in tectonite peridotites from the Maqsad district, Sumail ophiolite, southern Oman: Implications for the origin of the sulfide component in the oceanic upper mantle. Tectonophysics 151 (1-4), 57–73.

Lorand, J., Alard, O., 2010. Determination of selenium and tellurium concentrations in pyrenean peridotites (ariege, france): New insight into S/Se/Te systematics of the upper in mantle samples. Chemical Geology 278 (1), 120–130.

Lorand, J., Alard, O., Luguet, A., Keays, R., 2003. Sulfur and selenium systematics of the sub- continental lithospheric mantle: inferences from the Massif Central xenolith suite (France). Geochimica et Cosmochimica Acta 67 (21), 4137–4151.

Lorand, J., Luguet, A., Alard, O. 2013 Platinum-group element systematics and petrogenetic processing of the continental upper-mantle : a review. Lithos 164, 2-21

Luguet, A., Lorand, J., Alard, O., Cottin, J., 2004. A multi-technique study of platinum group element systematic in some Ligurian ophiolitic peridotites, Italy. Chemical geology 208 (1), 175–194.

Luguet, A., Lorand, J., Seyler, M., 2003. Sulfide petrology and highly siderophile element geochemistry of abyssal peridotites: a coupled study of samples from the kane fracture zone (45°W 23°20N, MARK area, atlantic ocean). Geochimica et Cosmochimica Acta 67 (8), 1553–1570.

Lynton, S., Candela, P., Piccoli, P., 1993. An experimental study of the partitioning of copper between pyrrhotite and a high silica rhyolitic melt. Economic Geology 88 (4), 901–915.

MacLean, W., Shimazaki, H., 1976. The partition of Co, Ni, Cu, and Zn between sulfide and silicate liquids. Economic Geology 71 (6), 1049–1057.

Maia, M., Hémond, C., Gente, P., 2001. Contrasted interactions between plume, upper mantle, and lithosphere: Foundation chain case. Geochemistry Geophysics Geosystems 2 (7), 1028–29.

Mandeville, C., Sasaki, A., Saito, G., Faure, K., King, R., Hauri, E., 1998. Open-system de- gassing of sulfur from Krakatau 1883 magma. Earth and Planetary Science Letters 160 (3-4), 709–722.

Mandeville, C., Webster, J., Tappen, C., Taylor, B., Timbal, A., Sasaki, A., Hauri, E., Bacon, C., 2009. Stable isotope and petrologic evidence for open-system degassing during the cli- mactic and pre-climactic eruptions of Mt. Mazama, Crater Lake, Oregon. Geochimica et Cosmochimica Acta 73 (10), 2978–3012.

Mathez, E., 1976. Sulfur solubility and magmatic sulfides in submarine basalt glass. Journal of Geophysical Research 81 (23), 4269–4276.

Mavrogenes, J., O'Neill, H., 1999. The relative effects of pressure, temperature and oxygen fugacity on the solubility of sulfide in mafic magmas. Geochimica et Cosmochimica Acta 63 (7-8), 1173–1180.

McDonough, W., 2003. Compositional model for the Earth's core. Treatise on geochemistry 2, 547–568.

McDonough, W., Sun, S., 1995. The composition of the Earth. Chemical Geology 120 (3-4), 223–253.

Métrich, N., Berry, A., O'Neill, H., Susini, J., 2009. The oxidation state of sulfur in synthetic and natural glasses determined by X-ray absorption spectroscopy. Geochimica et Cosmochimica Acta 73 (8), 2382–2399.

Michael, P., Cornell, W., 1998. Influence of spreading rate and magma supply on crystalliza- tion and assimilation beneath mid-ocean ridges: Evidence from chlorine and major element chemistry of mid-ocean ridge basalts. Journal of Geophysical Research 103 (B8), 18325–18.

Moore, J., Fabbi, B., 1971. An estimate of the juvenile sulfur content of basalt. Contributions to Mineralogy and Petrology 33 (2), 118–127.

Moore, J., Schilling, J., 1973. Vesicles, water, and sulfur in Reykjanes Ridge basalts. Contribu- tions to mineralogy and petrology 41 (2), 105–118.

Moreira, M., Kunz, J., Allègre, C., 1998. Rare gas systematics in popping rock: isotopic and elemental compositions in the upper mantle. Science 279 (5354), 1178–1181.

Moreira, M. A., Dosso, L., Ondréas, H., et al., 2008. Helium isotopes on the Pacific–Antarctic ridge (52.5–41.5 S). Geophysical Research Letters 35, L10306.

Niu, Y., Batiza, R., 1997. Trace element evidence from seamounts for recycled oceanic crust in the Eastern Pacific mantle. Earth and Planetary Science Letters 148 (3), 471–483.

Niu, Y., Regelous, M., Wendt, I., Batiza, R., O'Hara, M., 2002. Geochemistry of near-EPR seamounts: importance of source vs. process and the origin of enriched mantle component. Earth and Planetary Science Letters 199 (3), 327–345.

Oeser, M., Strauss, H., Wolff, P., Koepke, J., Peters, M., Garbe-Schonberg, D., Dietrich, M., 2012. A profile of multiple sulfur isotopes through the Oman ophiolite. Chemical Geology 312, 27–46.

Ohmoto, H., 1979. Isotope of sulfur and carbon. Geochemistry of Hydorothermal Ore Deposits, 509–567.

Ohmoto, H., Goldhaber, M., 1997. Sulfur and carbon isotopes. Geochemistry of hydrothermal ore deposits 3, 517–611.

Ondréas, H., Aslanian, D., Géli, L., Olivet, J., Briais, A., 2001. Variations in axial morphology, segmentation, and seafloor roughness along the pacific-antarctic ridge between 56 s and 66 s. J. geophys. Res 106, 8521–8546.

Ono, S., Keller, N., Rouxel, O., Alt, J., 2012. Sulfur-33 constraints on the origin of secondary pyrite in altered oceanic basement. Geochimica et Cosmochimica Acta.

Ono, S., Wing, B., Johnston, D., Farquhar, J., & Rumble, D., 2006. Mass-dependent fractionation of quadruple stable sulfur isotope system as a new tracer of sulfur biogeochemical cycles. Geochimica et Cosmochimica Acta, 70(9), 2238-2252.

Ono, S., Shanks, W., Rouxel, O., Rumble, D., 2007. S-33 constraints on the seawater sulfate contribution in modern seafloor hydrothermal vent sulfides. Geochimica et cosmochimica acta 71 (5), 1170–1182.

Otake, T., Lasaga, A., Ohmoto, H., 2008. Ab initio calculations for equilibrium fractionations in multiple sulfur isotope systems. Chemical Geology 249 (3), 357–376.

O'Neill, H., Mavrogenes, J., 2002. The sulfide capacity and the sulfur content at sulfide satura- tion of silicate melts at 1400° C and 1 bar. Journal of Petrology 43 (6), 1049–1087.

Palot, M., Cartigny, P., Harris, J. W., Kaminsky, F. V., & Stachel, T. 2012, Evidence for deep mantle convection and primordial heterogeneity from nitrogen and carbon stable isotopes in diamond. Earth and Planetary Science Letters, 357, 179-193.

Pedersen, A., 1979. Basaltic glass with high-temperature equilibrated immiscible sulphide bodies with native iron from Disko, central West Greenland. Contributions to Mineralogy and Petrology 69 (4), 397–407.

Peters, M., Strauss, H., Farquhar, J., Ockert, C., Eickmann, B., Jost, C., 2010. Sulfur cycling at the Mid-Atlantic Ridge: A multiple sulfur isotope approach. Chemical Geology 269 (3), 180–196.

Rai, V. K., & Thiemens, M. H., 2007. Mass independently fractionated sulfur components in chondrites. *Geochimica et cosmochimica acta*, *71*(5), 1341-1354.

Rajamani, V., Naldrett, A., 1978. Partitioning of Fe, Co, Ni, and Cu between sulfide liquid and basaltic melts and the composition of Ni-Cu sulfide deposits. Economic Geology 73 (1), 82–93.

32

Rees, C., Jenkins, W., Monster, J., 1978. The sulphur isotopic composition of ocean water sulphate. Geochimica et Cosmochimica Acta 42 (4), 377–381.

Rehkamper, M., Hofmann, A., 1997. Recycled ocean crust and sediment in Indian Ocean MORB. Earth and Planetary Science Letters 147, 93–106.

Richet, P., Bottinga, Y., Janoy, M., 1977. A review of hydrogen, carbon, nitrogen, oxygen, sulphur, and chlorine stable isotope enrichment among gaseous molecules. Annual Review of Earth and Planetary Sciences 5, 65–110.

Ripley, E., Brophy, J., Li, C., 2002. Copper solubility in a basaltic melt and sulfide liquid/silicate melt partition coefficients of cu and fe. Geochimica et cosmochimica acta 66 (15), 2791–2800.

Rose-Weston, L., Brenan, J., Fei, Y., Secco, R., Frost, D., 2009. Effect of pressure, temperature, and oxygen fugacity on the metal-silicate partitioning of Te, Se, and S: Implications for earth differentiation. Geochimica et Cosmochimica Acta 73 (15), 4598–4615.

Rouxel, O., Ono, S., Alt, J., Rumble, D., Ludden, J., 2008. Sulfur isotope evidence for microbial sulfate reduction in altered oceanic basalts at ODP Site 801. Earth and Planetary Science Letters 268 (1), 110–123.

Roy-Barman, M., Wasserburg, G., Papanastassiou, D., Chaussidon, M., 1998. Osmium isotopic compositions and re–os concentrations in sulfide globules from basaltic glasses. Earth and Planetary Science Letters 154 (1), 331–347.

Rubin, K., Sinton, J., Maclennan, J., Hellebrand, E., 2009. Magmatic filtering of mantle compositions at mid-ocean-ridge volcanoes. Nature Geoscience 2 (5), 321–328.

Saal, A., Hauri, E., Langmuir, C., Perfit, M., 2002. Vapour undersaturation in primitive mid- ocean-ridge basalt and the volatile content of earth's upper mantle. Nature 419 (6906), 451– 455.

Sakai, H., 1968. Isotopic properties of sulfur compounds in hydrothermal processes. Geochem. J 2 (1), 2.

Sakai, H., Casadevall, T., Moore, J., 1982. Chemistry and isotope ratios of sulfur in basalts and volcanic gases at Kilauea Volcano, Hawaii. Geochimica et Cosmochimica Acta 46 (5), 729–738.

Sakai, H., Marais, D., Ueda, A., Moore, J., 1984. Concentrations and isotope ratios of carbon, nitrogen and sulfur in ocean-floor basalts. Geochimica et Cosmochimica Acta 48 (12), 2433– 2441.

Seyler, M., Lorand, J., Dick, H., Drouin, M., 2007. Pervasive melt percolation reactions in ultra-depleted refractory harzburgites at the mid-atlantic ridge, 15°20 N: ODP Hole 1274A. Contributions to Mineralogy and Petrology 153 (3), 303–319.

Shanks, W. I., Bischoff, J., Rosenbauer, R., 1981. Seawater sulfate reduction and sulfur isotope fractionation in basaltic systems: Interaction of seawater with fayalite and magnetite at 200- 350 C. Geochimica et Cosmochimica Acta 45 (11), 1977–1995.

Shaw, A., Behn, M., Humphris, S., Sohn, R., Gregg, P., 2010. Deep pooling of low degree melts and volatile fluxes at the 85°E segment of the Gakkel ridge: evidence from olivine-hosted melt inclusions and glasses. Earth and Planetary Science Letters 289 (3-4), 311–322.

Sobolev, A., Hofmann, A., Kuzmin, D., Yaxley, G., Arndt, N., Chung, S., Danyushevsky, L., Elliott, T., Frey, F., Garcia, M., et al., 2007. The amount of recycled crust in sources of mantle-derived melts. Science 316 (5823), 412–417.

Taylor, B., 1986. Magmatic volatiles; isotopic variation of C, H, and S. Reviews in Mineralogy and Geochemistry 16 (1), 185–225.

Thirlwall, M., 1997. Pb isotopic and elemental evidence for OIB derivation from young HIMU mantle. Chemical Geology 139 (1), 51–74.

Thode, H., Monster, J., Dunford, H., 1961. Sulphur isotope geochemistry. Geochimica et Cos- mochimica Acta 25 (3), 159–174.

Vlastelic, I., Aslanian, D., Dosso, L., Bougault, H., Olivet, J., Geli, L., 1999. Large-scale chemical and thermal division of the Pacific mantle. Nature 399 (6734), 345–350.

Vlastelic, I., Dosso, L., Bougault, H., Aslanian, D., Géli, L., Etoubleau, J., Bohn, M., Joron, J., Bollinger, C., 2000. Chemical systematics of an intermediate spreading ridge: The Pacific- Antarctic Ridge between 56 degrees S and 66 degrees S. Journal Of Geophysical Research Solid Earth 105 (B2), 2915–2936.

Wallace, P., Carmichael, I., 1992. Sulfur in basaltic magmas. Geochimica et Cosmochimica Acta 56 (5), 1863–1874.

Wallace, P., Edmonds, M., 2011. The sulfur budget in magmas: Evidence from melt inclusions, submarine glasses, and volcanic gas emissions. Reviews in Mineralogy and Geochemistry 73, 215–246.

Wang Z., Becker H., 2013. Ratios of S, Se and Te in the silicate Earth require a volatile-rich late veneer. Nature 499, 328-

332.

Wedepohl, H., 1995. The composition of the continental crust. Geochimica et Cosmochimica Acta 59 (7), 1217–1232.

Willbold, M., Stracke, A., 2006. Trace element composition of mantle end-members: Implications for recycling of oceanic and upper and lower continental crust. Geochemistry Geophysics Geosystems 7 (4), Q04004.

Workman, R., Hart, S., 2005. Major and trace element composition of the depleted MORB mantle (DMM). Earth and Planetary Science Letters 231 (1), 53–72.

Young, E., Galy, A., Nagahara, H., 2002. Kinetic and equilibrium mass-dependent isotope fractionation laws in nature and their geochemical and cosmochemical significance. Geochimica et Cosmochimica Acta 66 (6), 1095–1104.

Figure caption:

Figure 1: Map showing the location of the 38 samples chosen for this study. Triangles are on-axis from the 66-56°S zone, circles are on-axis from the 53-41°S zone, and squares are off-axis from the 53-41°S zone. Locations of two major transform faults and the closest hotspots (Louisville and Foundation) are also shown

Figure 2: S abundance evolution across the magmatic differentiation. (A): S versus MgO abundances. (B): S versus FeO abundances. Theoretical prediction for S abundance evolution as modeled for a highly incompatible element (plain line) is also plotted.

Figure 3: (A): Cu abundances variations versus MgO for PAR basalts. MORB literature data are also plotted (grey circles). (B): Cu/Y ratios for the same samples. The black curve is modeled using equation 12 for a $D^{sulf-liq}_{Cu} = 900$ (Ripley et al., 2002)

Figure 4: (A): ^{34}S (B): •^{33}S (C): •^{36}S variations against dredging latitude of samples. ^{34}S range is 2.2‰, whereas the ^{34}S baseline is characterized by the lowest values, around -0.90‰. In contrast, •^{33}S and •^{36}S values displayed by samples are homogeneous with respect to typical uncertainties.

Figure 5: A: Cl versus K abundances for PAR basalts. B: Cl/K evolution with respect to MgO. In both diagrams, the uncontaminated basalt domain of Michael and Cornell (1998) is shown. Almost all samples display Cl excesses that are testimony of Cl-rich assimilation. This contamination process scales with magmatic differentiation, as shown by negative correlation between Cl/K and MgO.

Figure 6: V abundances versus MgO content for PAR basalts. Titano-magnetite appearance on the liquidus, occurring at MgO   5-6%, is likely responsible for the V drop in accordance with observations of Jenner et al. (2010) on MORB and back-arc melts.

Figure 7: ^{34}S of PAR basalts against their S remaining fraction (=f_{sulf}) as calculated using equation (1), see section 5.2. The black curve is calculated using equation As sulfide exsolution occurs under open system, it can be written:

$$d^{34}S_{residual} = d^{34}S_{initial} + 1000 \, \times \, \ln\left(^{34}a_{dissolved-exsolved}\right) \, \times \, \ln(f_{sulf}) \ (13)$$

and $\alpha_{dissolved-immiscible}$ can be suggested to be 1.00115, with a ^{34}S$_{initial}$ of -1.20‰. Isotope fractionation laws applied to ^{33}S and ^{36}S could give the opportunity to test this model. Under equilibrium and following the high-temperature approximation of Bigeleisen and Mayer (1947),

34

equation 13 can be applied to rare isotopes of sulfur, as $a_{dissolved\text{-}exsolved}^{3x/32} = \left(a_{dissolved\text{-}exsolved}^{34}\right)^{b}$. Under thermodynamic equilibrium,   is the ratio of reduced atomic masses of isotopes as follows:

$$b^{3x} = \frac{\dfrac{1}{m_{32}} - \dfrac{1}{m_{3x}}}{\dfrac{1}{m_{32}} - \dfrac{1}{m_{34}}}$$

[33] and [36] are hence defined at 0.5152 and 1.8889, respectively (Young et al., 2002). From mass balance conservation, mass-dependent fractionation leads to slight deviations from these theoretical arrays, which are enhanced by open system processing (Ono et al., 2006; Farquhar et al., 2007). Here, however, the expected $^{34}a_{dissolved\text{-}exsolved}$ is too close to 1.00 to allow significant deviations of both ^{33}S and ^{36}S with respect to theoretical curves: for initial •^{33}S and •^{36}S of +0.010‰ and -0.071‰ (see section 4), the predicted •^{33}S and •^{36}S at 20% remaining sulfur (i.e. 80% S lost by sulfide exsolution) are of +0.011‰ and -0.077‰ respectively, i.e. within uncertainty of the initial value (not shown). In other words, the multi-isotope composition of MORB cannot provide further constraint on the S isotope fractionation value accompanying the sulfide exsolution.

However, the scatter observed here is unreconcilable with a control of S isotope composition of melts via $^{34}S/^{32}S$ fractionation along Immiscible sulfide exsolution. For example, PAC1 DR11-1g glass is mildly differentiated (MgO = 6.93% and 76% remaining S). If its ^{34}S were only controlled by sulfide fractionation, it would be expected at -1.00 ± 0.15‰. Its ^{34}S is however determined at -0.29 ± 0.03‰, significantly offset from its predicted value. The same conclusion can be drawn with PAC2 DR25-1 off-axis glass: its remaining S fraction is calculated at 80% (i.e. among the least sulfide-fractionated sample, Table 3) but its ^{34}S is determined at +0.35 ± 0.05‰, significantly offset from its predicted value of -1.00 ± 0.15‰. It is acknowledged that if the melting degree decreases (i.e. the fraction of dissolved S decreases), the melt ^{34}S increases. Whereas major element melting extent proxies such as $Na_{8.0}$ (Klein and Langmuir, 1987; Vlastelic et al., 2000; Hamelin et al., 2010; Clog et al; 2013) do not point toward such variation, the magnitude of $^{34}S/^{32}S$ fractionation here allows at most +0.5‰ deviation, failing to explain the observed scatter at a given f_{sulf}.

Figure 8: ^{34}S variation as a function of Cl/K ratios of PAR basalts. Two subsets of samples are apparent: A first group displays positive trend between ^{34}S and Cl/K (n=10) whereas the other exhibits no trend between these parameters (n=28), for comparable Cl/K range.

Figure 9: $^{206}Pb/^{204}Pb$ ratios (Hamelin et al., 2011) for all samples and ^{34}S variation for non-contaminated samples along ridge axis are presented against basalt location. Average ^{34}S values are calculated on on-axis basalts.

Figure 10: ^{34}S variations as a function of $^{206}Pb/^{204}Pb$. Two distinct trends for two geographic locations are apparent. Black curves are calculated using mixing between DM and HIMU-S as well as HIMU-N. The model allows an identical ^{34}S for HIMU-S and -N of +3.00‰ with 300 and 175 ppm S, respectively. ^{34}S of DM is taken at -1.40 ± 0.50‰.

Figure 11: •^{33}S variations as a function of ^{34}S for PAR non-contaminated basalts. The lack of •^{33}S significant variability constrain the •^{33}S of the extreme endmember between -0.050 and +0.050‰. Two models based on Cabral et al., (2013) estimate for HIMU are presented: Variability displayed by the studied samples point toward a composition being significantly distinct of the Cabral et al, (2013) estimate of •^{33}S = -0.400‰ for the HIMU endmember, independently of HIMU $\delta^{34}S$. See main text for discussion.

35

Table 1: Locations and dredging depths for the 38 sample analyzed in this study

Table 2: Multiple sulfur isotope composition of the 38 basalts studied in this report

Table 3: S, Cu and Cl abundances of the studied samples. (a): Ratio calculated using yttrium data of Hamelin et al. (2010). (b): Cu and Cl abundances determined using electron microprobe with a typical standard deviation of 8 and 10 ppm, respectively.

Table 4: Major element composition of studied off-axis basalts determined with electron microprobe under standard procedure.

Table 5: S abundance and isotope parameters of contamination models. For the MORB endmember, $\Delta^{33}S$ and $\Delta^{36}S$ values are chosen as the PAR average (this study), whereas $\delta^{34}S$ is taken as close to the non-contaminated average. Small variation of the chosen $\delta^{34}S$ for the MORB endmember does not impact the result of the modeling.

Table 6: Parameters of the two-component PAR mantle source. HIMU-S is HIMU South of 45°85' S, and HIMU-N is HIMU North of 45°85'S. (a): Workman and Hart (2005). (b): Jackson and Dasgupta (2008). (c): Inferred after Kelley et al., (2005), see main text for details

Table 7: Abundances and isotope composition of sulfur in the depleted mantle and in complementary surface reservoirs. (a): Rees (1978). (b): Alt (1995). (c): Wedepohl (1995).

sample	Latitude (°N)	Longitude (°E)	Depth (m)
On-axis basalts dredged on the Pacific-Antarctic ridge			
PAC1 CV02-g	-64.834	172.428	2936
PAC1 CV03-g	-64.533	171.875	2576
PAC1 CV04-g	-64.399	169.400	2340
PAC1 DR05-1g	-62.000	154.538	2344
PAC1 DR06-g	-60.935	153.212	2527
PAC1 DR07-1g	-59.996	152.078	2362
PAC1DR10-1g	-57.892	148.498	2319
PAC1 DR11-1g	-57.633	146.798	2500
PAC1 DR12-1g	-57.180	146.286	2539
PAC1 DR13-2	-56.570	145.743	2674
PAC2 DR01-1	-52.525	118.345	2323
PAC2 DR02-1	-52.127	118.133	2405
PAC2 DR04-2	-51.425	117.775	2409
PAC2 DR05-02g	-50.975	117.403	2784
PAC2 DR06-6	-50.698	117.192	2610
PAC2 DR08-1	-49.992	116.965	2221
PAC2 DR20-1	-49.733	113.783	2441
PAC2 DR21-2	-49.255	113.598	2339
PAC2 DR22-1	-48.725	113.365	2413
PAC2 DR27-1	-48.182	113.342	2359
PAC2 DR28-2	-47.505	113.250	2489
PAC2 DR29-1	-47.005	113.085	2407
PAC2 DR30 1	-46.400	112.873	2345
PAC2 DR31-3	-45.850	112.693	2414
PAC2 DR32-1	-45.393	112.432	2384
PAC2 DR33-1	-44.872	112.253	2374

PAC2 DR34-1	-44.237	112.035	2467
PAC2 DR36-1	-42.947	111.555	2503
PAC2 DR37-2	-42.273	111.335	2475
PAC2 DR38-1	-41.800	111.273	2524
Off-axis basalts dredged on seamounts near the Pacific-Antarctic ridge			
PAC2 DR16-7	-50.197	115.890	1700
PAC2 DR16-1	-50.197	115.890	1700
PAC2 DR11-3	-50.065	116.470	2300
PAC2 DR26-3	-48.615	115.260	1190
PAC2 DR25-1	-48.610	114.787	2000
PAC2 DR42-1c	-41.928	112.162	1480
PAC2 DR39-4	-41.253	113.685	2050
PAC2 DR43-1	-40.535	111.033	1600

sample	d34S V-CDT (‰)	d34S 1s (‰)	D33S CDT (‰)	D33S 1s (‰)	D36S CDT (‰)	D36S 1s (‰)
On-axis basalts dredged on the Pacific-Antarctic ridge						
PAC1 CV02-g	-0.91	0.14	0.000	0.003	-0.070	0.040
PAC1 CV03-g	-0.72	0.02	0.005	0.001	-0.043	0.039
PAC1 CV04-g	-0.83	0.04	0.002	0.005	-0.005	0.021
PAC1 DR05-1g	-0.94		-0.001		-0.044	
PAC1 DR06-g	-0.89	0.05	0.006	0.003	-0.027	0.091
PAC1 DR07-1g	-0.95	0.01	0.009	0.003	-0.120	0.008
PAC1DR10-1g	-0.14	0.03	0.004	0.004	-0.001	0.037
PAC1 DR11-1g	-0.29	0.03	-0.001	0.001	0.001	0.141
PAC1 DR12-1g	-0.31	0.01	0.003	0.004	0.032	0.074
PAC1 DR13-2	-0.65	0.10	0.004	0.004	-0.114	0.013
PAC2 DR01-1	-0.81	0.14	0.002	0.004	0.019	0.033
PAC2 DR02-1	-0.10	0.09	-0.003	0.007	-0.050	0.064

PAC2 DR04-2	-0.80		0.003		-0.061	
PAC2 DR05-02g	-0.78	0.04	-0.001	0.001	-0.031	0.040
PAC2 DR06-6	-0.14		-0.009		-0.079	
PAC2 DR08-1	-0.77	0.02	0.003	0.006	-0.071	0.018
PAC2 DR20-1	0.60	0.10	0.003	0.008	-0.025	0.065
PAC2 DR21-2	-0.42	0.03	0.004	0.006	-0.061	0.033
PAC2 DR22-1	-0.83	0.05	-0.005	0.004	0.066	0.095
PAC2 DR27-1	-0.10	0.08	-0.004	0.011	-0.026	
PAC2 DR28-2	-0.80	0.01	0.003	0.001	0.045	
PAC2 DR29-1	-0.20	0.01	0.006	0.001	-0.040	0.045
PAC2 DR30 1	-0.72		0.004		0.003	
PAC2 DR31-3	-1.02	0.01	0.003	0.001	-0.023	0.041
PAC2 DR32-1	-0.70	0.04	-0.002	0.001	-0.013	0.106
PAC2 DR33-1	-0.86	0.01	0.000	0.004	-0.134	0.066
PAC2 DR34-1	-0.99	0.30	-0.007	0.01	-0.03	0.08

				6	5	6
PAC2 DR36-1	-1.11	0.08	0.002	0.001	-0.050	0.042
PAC2 DR37-2	-1.00	0.10	0.006	0.002	-0.016	0.022
PAC2 DR38-1	-1.12	0.02	0.005	0.008	-0.028	0.020
Off-axis basalts dredged on seamounts near the Pacific-Antarctic ridge			0.017			
PAC2 DR16-7	-0.72	0.02	-0.004	0.004	-0.036	0.080
PAC2 DR16-1	-0.82	0.16	0.005	0.007	-0.099	0.080
PAC2 DR11-3	-0.70		0.011		-0.011	0.080
PAC2 DR26-3	-0.75	0.11	0.009	0.001		
PAC2 DR25-1	0.35	0.06	-0.004	0.001	-0.046	0.008
PAC2 DR42-1c	-1.57	0.11	0.006	0.008	-0.125	0.080
PAC2 DR39-4	-1.25		-0.010		0.029	0.080
PAC2 DR43-1	-1.13	0.06	0.009	0.004		

sample	S (ppm)	S 1s (ppm)	f sulf	Cl (ppm)	Cl/K	Cu (ppm)	Cu/Y
On-axis basalts dredged on the Pacific-Antarctic ridge							
PAC1 CV02-g	1171	50	0.71	49	0.10	57	1.56
PAC1 CV03-g	938	42	0.82	38	0.06	72	3.01
PAC1 CV04-g	940	52	0.85	75	0.22	85	3.68
PAC1 DR05-1g	932	40	0.80	47	0.06	85	3.35
PAC1 DR06-g	1351	48	0.68	290	0.29	57	1.35
PAC1 DR07-1g	1301	33	0.67	494	0.31	69	1.73
PAC1DR10-1g	1047	39	0.23	2163	0.54	68	0.96
PAC1 DR11-1g	1153	44	0.76	162	0.32	76	2.63
PAC1 DR12-1g	968	26	0.89	36	0.14	82	3.43
PAC1 DR13-2	1259	84	0.69	75	0.10	64	1.82
PAC2 DR01-1	1116	36	0.70	225	0.13	82	2.12
PAC2 DR02-1	1429	48	0.64	616	0.37	62	1.35
PAC2 DR04-2	1199	24	0.66	264	0.26	65	1.50
PAC2 DR05-02g	1339	47	0.58	292	0.19	66	1.33
PAC2 DR06-6	1630	30	0.31	1426	0.55	54	0.57
PAC2 DR08-1	123	57	0.6	266	0.1	88	2.4

42

	9		2		6		6
PAC2 DR20-1	1550	50	0.32	1475	0.71	52	0.59
PAC2 DR21-2	1312	105	0.64	287	0.23	62	1.40
PAC2 DR22-1	1172	39	0.66	281	0.20	76	1.78
PAC2 DR27-1	1755	14	0.35	1047	0.24	29	0.40
PAC2 DR28-2	1112	44	0.73	223	0.33	93	2.86
PAC2 DR29-1	1471	32	0.59	404	0.25	71	1.39
PAC2 DR30 1	1348	21	0.68	373	0.26	69	1.53
PAC2 DR31-3	1208	37	0.71	435	0.52	73	1.77
PAC2 DR32-1	1321	41	0.64	335	0.25	66	1.47
PAC2 DR33-1	1340	25	0.62	277	0.22	63	1.35
PAC2 DR34-1	1094	22	0.79	77	0.15	74	2.33
PAC2 DR36-1	1381	32	0.70	514	0.41	67	1.37
PAC2 DR37-2	1435	16	0.93	441	0.48	60	1.24
PAC2 DR38-1	1244	36	0.91	141	0.19	67	2.04
Off-axis basalts dredged on seamounts near the Pacific-Antarctic ridge							
PAC2 DR16-7	739	40	0.66	82	0.09	35	2.00
PAC2 DR16-1	758	40	0.67	41	0.04	35	2.00
PAC2 DR11-3	1101	16	0.84	142	0.09	79	2.78

PAC2 DR26-3	1009	40	0.94	56	0.11	79	3.49
PAC2 DR25-1	1140	18	0.79	343	0.33	91	3.55
PAC2 DR42-1c	867	40	0.86	25	0.05	112	6.32
PAC2 DR39-4	1029	15	0.76	23	0.05	109	4.32
PAC2 DR43-1	966	40	0.95	56	0.11	56	2.45

	Na2O	SiO2	K2O	Al2O3	CaO	MgO	P2O5	FeO	MnO	TiO2	206Pb/204Pb
PAC2 DR16 -7	2.87	52.39	0.11	16.22	9.50	7.84	0.20	7.95	0.13	1.21	19.012
PAC2 DR16 -1	2.82	52.20	0.11	16.12	9.50	8.02	0.20	7.98	0.13	1.20	19.012
PAC2 DR11 -3	2.85	49.31	0.12	14.83	12.11	7.77	0.42	9.34	0.17	1.41	18.746
PAC2 DR26 -3	2.93	49.11	0.09	16.42	11.08	8.18	0.18	8.89	0.16	1.25	18.560
PAC2 DR25 -1	3.14	49.26	0.08	15.66	11.87	7.95	0.41	9.37	0.14	1.41	18.777
PAC2 DR42 -1c	2.25	46.76	0.03	17.51	11.44	9.32	0.12	9.69	0.18	0.80	18.783
PAC2 DR39 -4	2.86	49.08	0.05	15.55	9.64	8.86	0.31	11.89	0.18	1.35	19.537
PAC2 DR43 -1	2.34	49.45	0.05	16.32	11.95	8.93	0.16	8.16	0.15	0.97	18.741

	MORB	contaminant I	contaminant II
S abundance (wt %)	0.1	1	3
d34S (‰)	-1	5	10
D33S (‰)	0.01	0.018	0.018
D36S (‰)	-0.076	-0.126	-0.126

	DM	HIMU-S	HIMU-N
d34S (‰)	-1.4	3.0	3.0
206Pb/204Pb	17.573[a]	21.199[b]	21.199[b]
S (ppm)	200	300	175
Pb (ppm)	0.014[a]	0.064[c]	0.064[c]
S/Pb	14286	4651	2713

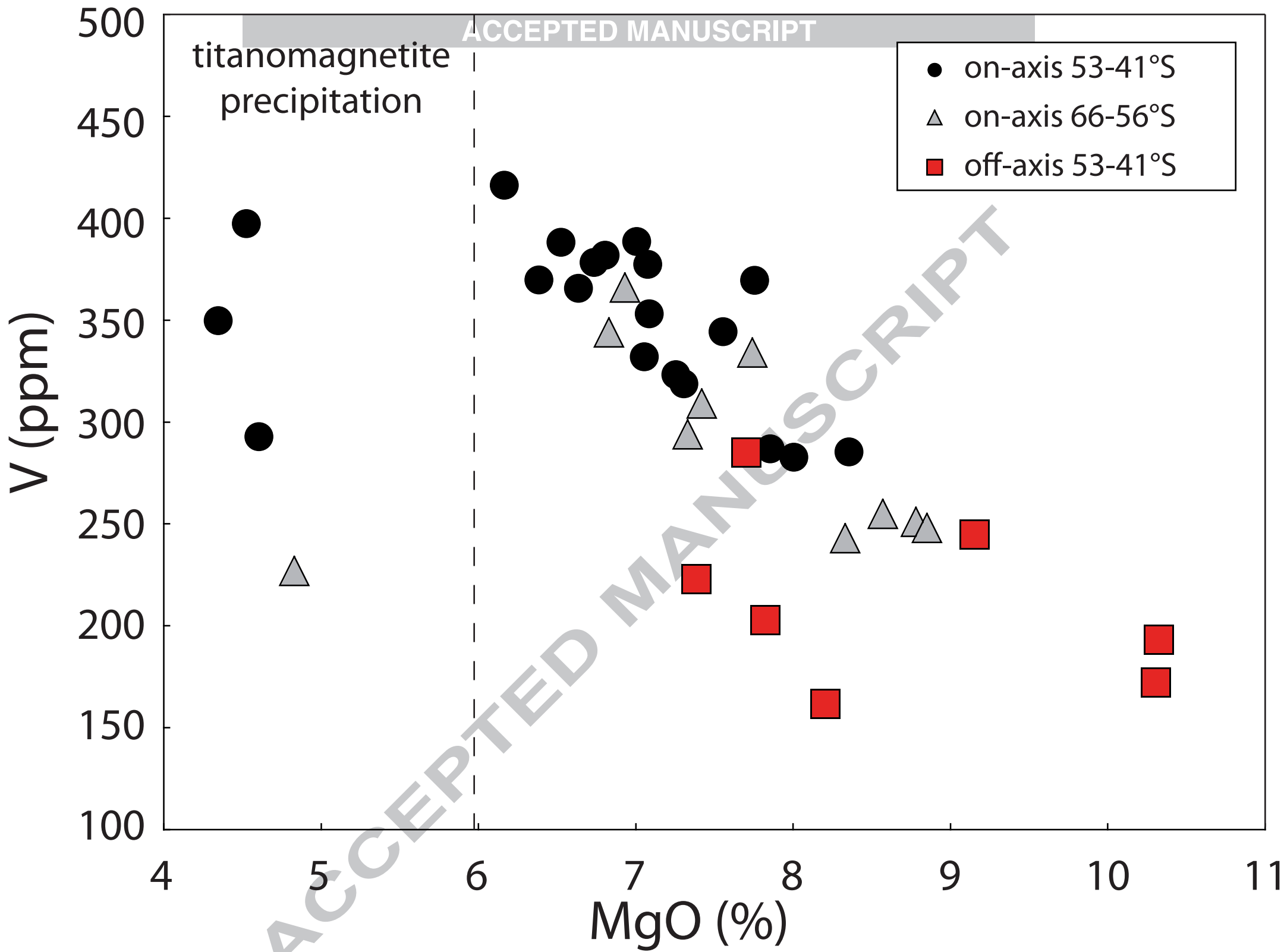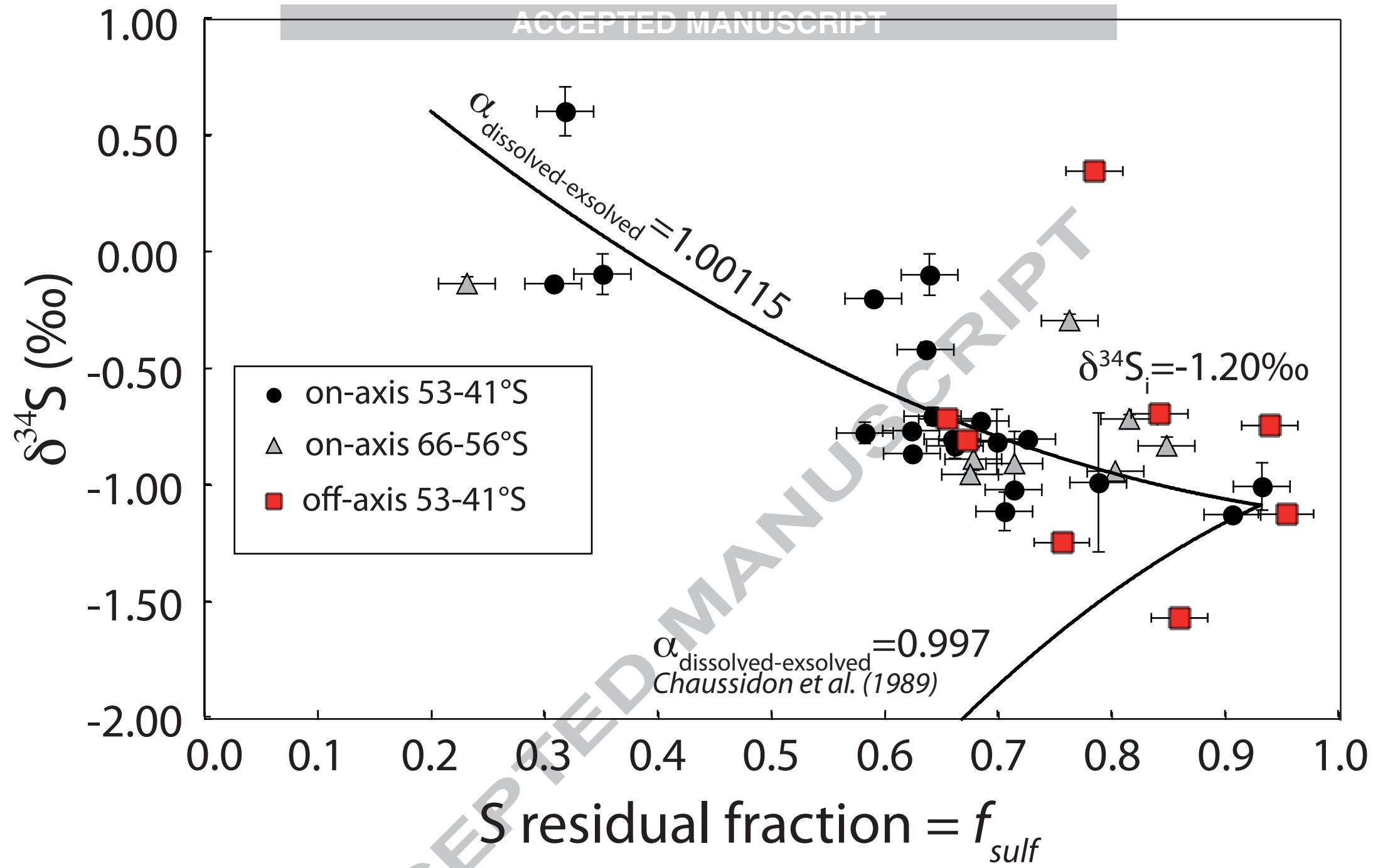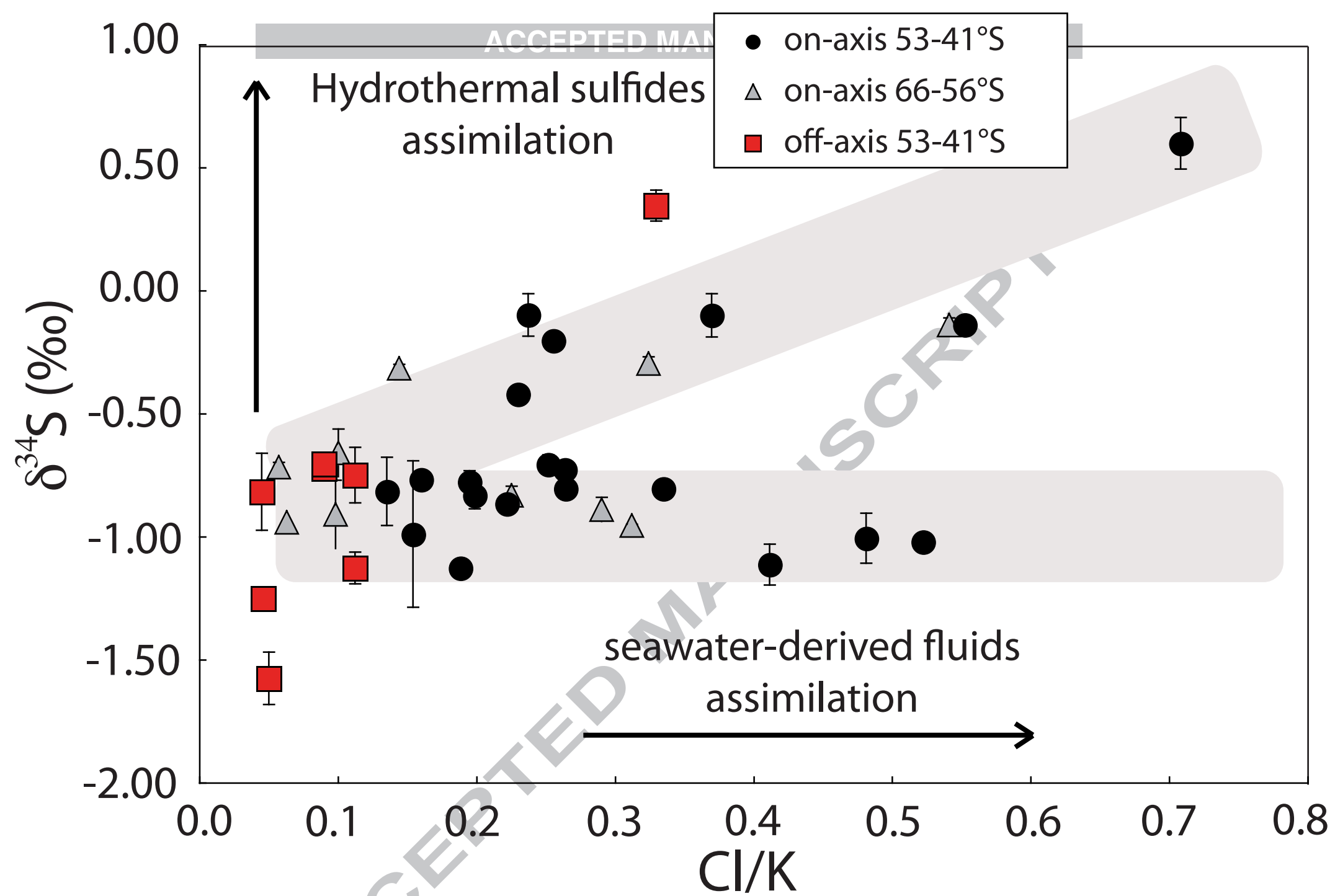| reservoir	mass (g)	S abundance (ppm)	S mass (g)	Contribution to the bulk S (%)	d34S (‰)
parent body of the Earth, following Gao and Thiemens (1993a,b)					
Ordinary chondrites					0.04
Carbonecous chondrites					0.32
enstatite chondrites					-0.26
weighed mean					0.04
Mass balance of terrestrial reservoir for a Sm/Nd chondritic Earth, following DePaolo (1980)					
Ocean	1.35×10^{24}	915[a]	1.24×10^{21}	0.56	21.00[a]
Oceanic crust	6.00×10^{24}	940[b]	5.64×10^{21}	2.56	2.70[b]
Continental Crust	1.90×10^{25}	697[c]	1.32×10^{22}	6.02	-1.66[c]
Sub-total	2.64×10^{25}	764	2.01×10^{22}	9.14	-1.63
DM + recycled oceanic crust	1.00×10^{27}	200	2.00×10^{23}	90.86	-0.89
Total	1.03×10^{27}	214	2.20×10^{23}	100	-0.72
Mass balance of terrestrial reservoir for a Sm/Nd chondritic Earth, following DePaolo (1980)					
Ocean	1.35×10^{24}	915[a]	1.24×10^{21}	0.19	21.00[a]
Oceanic crust	6.00×10^{24}	940[b]	5.64×10^{21}	0.85	2.70[b]
Continental Crust	1.90×10^{25}	697[c]	1.32×10^{22}	2.01	-1.66[c]
Sub-total	2.64×10^{25}	764	2.01×10^{22}	3.05	-1.63
DM + recycled oceanic crust	3.20×10^{27}	200	6.40×10^{23}	96.95	-0.89
Total	3.23×10^{27}	205	6.60×10^{23}	100	-0.83

A

Legend:
- on-axis ; 53-41°S (black circle)
- on-axis ; 66-56°S (gray triangle)
- off-axis ; 53-41°S (red square)
- MELTs prediction for $D_{sil-melt} = 10^{-3}$ (blue line)

1σ uncertainty

B

1σ uncertainty